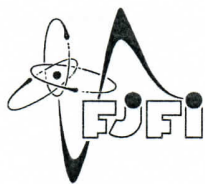


Czech Technical University in Prague
Faculty of Nuclear Sciences and Physical Engineering
Department of Physical Electronics

Thulium-doped fiber amplifier

Master's thesis

Author: **Bc. Jan Pokorný**
Supervised by: **doc. Ing. Pavel Peterka, Ph.D.**
Consultants: **prof. Dr. Ing. Ivan Richter**
Academic year: **2022/2023**



ČESKÉ VYSOKÉ UČENÍ TECHNICKÉ V PRAZE
FAKULTA JADERNÁ A FYZIKÁLNĚ INŽENÝRSKÁ
Katedra fyzikální elektroniky

ZADÁNÍ DIPLOMOVÉ PRÁCE

Student: **Bc. Jan P o k o r n ý**

Studijní program: **Fyzikální elektronika**

Specializace: **Fotonika**

Akademický rok: **2022/2023**

Název práce: **Thuliem dopovaný vláknový zesilovač**
(česky)

Název práce: **Thulium-doped fiber amplifier**
(anglicky)

Jazyk práce: **Angličtina**

Cíl práce:

Cílem je sestavení a charakterizace vláknového zesilovače pro vlnové délky ze spektrální oblasti nacházející se za telekomunikačním L-pásmem (1565-1625 nm), které budou využívat jako zesilovací médium thuliem dopovaná optická vlákna vyrobená v Ústavu fotoniky a elektroniky AV ČR (ÚFE) [1]. V zesilovači bude studována možnost posunutí pásma zesílení směrem ke kratším vlnovým délkám (<1850 nm) díky ohybu vlákna a vhodně navrženého profilu indexu lomu vlákna.

Pokyny pro vypracování

1. Seznamte se s možnostmi zesilování signálu ve spektrálním rozsahu ležícím za telekomunikačním L-pásmem (1565-1625 nm) pomocí optických vláknových zesilovačů [2, 3] a s možnostmi potlačení zesílené spontánní emise v dlouhovlnné části emisního spektra lanthanoidů vlnovodnými vlastnostmi optických vláken s poklesem indexu lomu v prstenci kolem jádra vlákna [4, 5].
2. Navrhněte a sestavte přeladitelný vláknový laser za účelem měření zesílení vláknových zesilovačů. Proveďte charakterizaci rozsahu jeho spektrální přeladitelnosti, tvaru spektra, výkonových charakteristik a časového průběhu signálu
3. Proveďte měření spektrálního útlumu optických vláken s potlačeným indexem lomu v prstenci kolem jádra vlákna v závislosti na poloměru ohybu vlákna.
4. Navrhněte a sestavte thuliem dopovaný vláknový zesilovač a změřte spektrální průběh zesílení. Proměřte spektrální zesílení vláknového zesilovače s thuliem dopovaným vláknem

navrženým pro posunutí zesílení ke kratším vlnovým délkám. Diskutujte vliv ohybu a tvaru profilu indexu lomu vlákna na posun spektrálního průběhu zesílení.

Doporučená literatura:

1. Koška P., Peterka P., Aubrecht J., Podrazký O., Todorov F., Becker M., Baravets Y., Honzátko P., and Kašík I., Enhanced pump absorption efficiency in coiled and twisted double-clad thulium-doped fibers, *Opt. Express* 24, 102-107, 2016.
2. Petrovich M. N., Poletti F., Wooler J. P., et al. Demonstration of amplified data transmission at 2 μm in a low-loss wide bandwidth hollow core photonic bandgap fiber, *Opt. Express* 21(23), 28559-28569, 2013.
3. Jung Y., Li Z., Simakov N., Daniel J. M. O., Jain D., Shardlow P. C., Heidt A. M., Sahu J. K., Hemming A., Clarkson W. A., Alam S. U., and Richardson D. J., Silica-based thulium doped fiber amplifiers for wavelengths beyond the L-band, in *Proc. Optical Fiber Communication Conference, Anaheim, California, M3D.5*, 2016.
4. Thyagarajan K., Kakkar C, S-band single-stage EDFA with 25-dB gain using distributed ASE suppression, *IEEE Photonics Technology Letters*. 16, 2448–2450, 2004.
5. Yeh C.-H., Lee C.-C., Chi S., A tunable S-band erbium-doped fiber ring laser, *IEEE Photonics Technology Letters* 15, 1053–1054, 2003.

Jméno a pracoviště vedoucího práce:

doc. Ing. Pavel Peterka, Ph.D.

Ústav fotoniky a elektroniky Akademie věd ČR, v.v.i.

Jméno a pracoviště konzultanta:

doc. Dr. Ing. Ivan Richter

Katedra fyzikální elektroniky, Fakulta jaderná a fyzikálně inženýrská ČVUT v Praze

Datum zadání: 10. říjen 2022

Datum odevzdání: 3. květen 2023

Doba platnosti zadání je dva roky od data zadání.

P. Peterka

Garant programu

P. Richter

Vedoucí katedry

I. Richter

Děkan

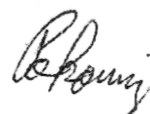


Prohlášení

Prohlašuji, že jsem předloženou práci vypracoval samostatně a že jsem uvedl veškerou použitou literaturu.

V Praze dne 2.5.2023

Jan Pokorný

Handwritten signature of Jan Pokorný in black ink.

Acknowledgements

I would like to thank my colleagues at the Institute of Photonics and Electronics, namely doc. Ing. Pavel Peterka, Ph.D. for his professional supervision and valued advice, Ing. Jan Aubrecht, Ph.D. for his time and cooperation on many aspects of this thesis, Ing. Yauhen Baravets, Ph.D. for his help with the tunable laser source and Bc. Bára Jiříčková for her assistance in measurement campaigns. I would also like to thank doc. Ing. Matěj Komanec, Ph.D. and the Faculty of Electrical Engineering of the Czech Technical University in Prague for providing the Yokogawa AQ6375B OSA and allocating lab time for our experiments. This work was financially supported by the Development Fund of CESNET under project number 672/2021.

Jan Pokorný

Contents

1	Introduction	8
2	Thulium doped amplifiers for telecom applications	10
3	Depressed-cladding fiber	14
3.1	Background	14
3.2	Simulation	14
3.3	Fiber manufacturing	16
4	Amplifier characterization methods	18
4.1	Gain	18
4.2	Noise Figure	20
4.2.1	Intensity noise	21
4.2.2	Noise figure definition	22
4.2.3	Noise factor of an optical cascade	24
4.2.4	The optical method	25
4.2.5	Source subtraction technique	26
4.2.6	Polarization extinction technique	27
5	SG1797 TDF attenuation measurement	29
6	TTDFL experimental setup	32
6.1	TTDFL-S experimental setup	32
6.2	TTDFL-L experimental setup	33
6.3	TTDFL characterization	34
7	TDFA experimental setup	35
7.1	TDFA-S-790 experimental setup	35
7.2	TDFA-S-1565 experimental setup	36
7.3	TDFA-L experimental setup	37

7.4	TDFA characterization	39
8	Results and discussion	41
8.1	TTDFL-S results	41
8.2	TTDFL-L results	44
8.3	TDFA-S-790 results	47
8.4	TDFA-S-1565 results	48
8.5	TDFA-L results	49
8.6	Combining the setups	52
9	Conclusions	53
	List of Figures	54
	References	56
	Abstract	63
	Abstrakt (Czech)	64
	Appendices	65
A	SPIE Photonics Europe 2022 Proceedings Article	i
B	SPIE Optics + Optoelectronics 2023 Proceedings Article	ix
C	CLEO/Europe-EQEC 2023 Contribution	xvi

1 Introduction

The invention of broadband optical amplifiers has been a key driver in advancement of global communication networks for the past decades. The ability to amplify optical signals travelling through low loss silica optical fibers without the need to electronically receive and retransmit them has become ever important in the modern information-based society as the demand for more data throughput continues to grow. Erbium-doped fiber amplifiers (EDFA) see particular use in this area as their gain bandwidth corresponds particularly well with the low loss transmission window of silica optical fibers. As is often the case, every new technology eventually reaches its limits and existing optical communication infrastructure is already approaching its physical limits due to an exponential rise of data traffic over the years [1] and simply adding more and more physical connections isn't a viable option. The focus has, for the most part, been on improving upon existing technology and utilizing the available bandwidth in the most efficient way. Recent technological advances provide another avenue of data transmission rate growth by expanding the available bandwidth. The E-band (1360-1460 nm) and S-band (1460-1530 nm) are being examined for use with existing fiber optic networks utilizing semiconductor optical amplifiers [2]. Upgrading existing 1.3 μm telecommunication links in the O-band (1260-1360 nm) using bismuth-doped fiber amplifiers can also become an attractive option [3]. The spectral region beyond the L-band (1565-1625 nm), which may soon become viable for data transmission due to the development of low-loss anti resonant hollow-core optical fibers (AR-HCF) [4], also shows a lot of potential in this area. AR-HCFs are a promising new breed of optical fibers that offer low transmission losses across a wide spectral range [5] including the L-band and beyond as well as reduced latency and a host of other benefits associated with utilizing a hollow core compared to existing systems. Indeed, lower loss than that of the best single mode silica optical fibers, which have been perfected for years, has recently been achieved. The next logical step is to develop optical fiber amplifiers, covering the newly viable spectral regions, ideally with similar or better performance characteristics than that of existing ones. Thulium-doped fiber amplifiers (TDFA) are of particular interest for application in

the spectral region beyond the L-band showing promising results [6, 7]. TDFAs offer the widest gain band (window from ~ 1750 to ~ 2050 nm) [8] amongst all rare earth doped fiber amplifiers providing further potential means to expand the overall fiber capacity. Thulium-doped fibers (TDF) yield fluorescence spanning the band from 1600 to 2200 nm and hence are an attractive gain medium for power scalable laser sources operating in this eye-safe wavelength range. The current silica TDFs, usually prepared by the well-established modified chemical vapor deposition (MCVD) method extended by solution doping techniques [9] or the innovative nanoparticle doping [10–14] technique, reach fluorescent lifetimes of almost 800 μs [11, 15] enhancing efficiency in various applications. Further applications of TDFAs may include free-space optical communication [16], LIDAR based gas sensing [17], material processing [18], polymer welding [19], pumping of solid-state lasers and generation of supercontinuum [20], optical coherence tomography [21], defense applications [22], or medical applications [23]. The goal of this work is to develop TDFAs for optical signal amplification in the spectral region beyond the L-band for telecom use.

2 Thulium doped amplifiers for telecom applications

TDFAs have long been a subject of interest in the field of optical telecommunication. The intended coverage has, however, changed over the years. The need to cover the low-loss region of silica optical fibers in the S-band (1480-1530 nm) has aroused interest in gain-shifted TDFAs in the early 2000s. In 2001 Kasamatsu et al. presented a gain shifted TDFA with high optical efficiency of 29% and high output power of 21.5 dBm. The gain shifted TDFA operated in the 1480-1510 nm waveband by employing a, at the time novel, diode pumping scheme at 1.4 and 1.56 μm [24]. The relatively recent advent of AR-HCFs has sparked a new wave of interest in TDFAs as they are ideal candidates for signal amplification in the 1650-2050 nm waveband. The relatively high attenuation of standard silica based optical fibers beyond 1600 nm as well as larger bend radii required for signal retention has so far made transmission at longer wavelengths over long distances using existing telecom networks unfeasible. Should the development of AR-HCFs succeed as envisioned, TDFAs may become the key enablers in next generation telecom networks. While AR-HCFs are being perfected, another potential application of TDFAs in the 1650-2050 nm waveband is feasible using existing silica fiber technology for medium distance communication i.e., across data centers, where high signal attenuation can be somewhat neglected. Several notable contributions have been published in the recent years paving the way for future developments. In 2013 Li et al. published the first in-band diode pumped TDFAs operating in the 2 μm waveband and demonstrated amplification over a 240 nm wide window in the range 1810-2050 nm with gain up to 36 dB and noise figure as low as 4.5 dB. The amplifier employs a commercially available core pumped TDF and commercially available laser diodes (LD) emitting at 1550 nm. The authors note that amplifier characteristics can be further improved by optimizing the various optical components. The gain at the edges of amplification range can be adjusted by varying the length of the active fiber. The authors conclude that TDFAs are certainly a feasible option for 2 μm optical communication [25]. In the same year Li et al. published an in-band EDFL pumped TDFA of two different designs, optimized for short and long wavelength operation, delivering maximum

small signal gain of 45 dB at 1950 nm and a relatively flat gain characteristic of more than 35 dB over a 90 nm bandwidth (1910-2000 nm). High power operation with output signal power of more than 1.2 W was also demonstrated. The amplifier employed a commercially available core pumped TDF. The long wavelength optimized TDFA employed an indirectly pumped section of TDF, which served to enhance gain at longer wavelengths, a trick used similarly in L-band EDFAs. The authors highlight other potential applications of TDFAs, mainly in optical sensing and medical applications [16]. Those contributions address amplification in the 2 μm waveband, where the reabsorption from the Tm^{3+} ions is relatively small. The 1650-1800 nm waveband is problematic in this sense as high inversion of population in the TDF is required in order to prevent signal reabsorption. The first demonstration of a silica based TDFA operating in the 1650-1700 nm waveband was published by Li et al. in 2015. Up to 29 dB small signal gain and noise figure as low as 6.5 dB was achieved. A commercially available core pumped TDF was used as a gain medium. An in-house built EDFL was used as an in-band pump. Special consideration was given to ASE generation in the TDF, which must be suppressed in order to maintain high inversion in the active fiber. A dispersion compensating fiber was inserted and bent in a small radius to induce high losses (>20 dB at 1720 nm, no transmission at >1750 nm) at longer wavelengths to suppress ASE generation and parasitic lasing. The authors note that amplifier characteristics can be substantially improved by using more optimized optical components and distributed ASE filtering [26]. Further enhancements to gain bandwidth of TDFAs can be achieved for example by multi-wavelength pumping as presented by Wang et al. in 2016. The presented amplifier combined 791 nm, 1240 nm and 1560 nm laser diode pumping and reached $\sim 47\%$ improvement in gain bandwidth compared to single wavelength pumping in 1.7-1.9 μm waveband. A 15 dB gain spanning 250 nm in the 1700-1950 nm waveband with a maximum gain of 29 dB and noise figure of less than 5 dB was presented. Notable is the increase in shorter wavelength gain when 791 nm pumping is used on top of 1560 nm pumping, on the other hand, adding 1240 nm pumping on top of the previously mentioned increases the gain bandwidth at longer wavelengths. The authors note that the added system complexity of employing 1240 nm

pumping for a triple wavelength pumping scheme is generally not worth the gain bandwidth enhancement it provides. The TDF used in the setup is a commercially available core pumped TDF [6]. In 2016 Jung et al. presented a more encompassing solution for amplification in the 1650-2050 nm band. The authors combined several TDFAs optimized for short, central and long wavelength operation. By combining the gain curves of the three optimized designs a gain of >20 dB and noise figure 5-10 dB over the 1650-2050 nm waveband has been achieved. A combination of previously demonstrated techniques was used to optimize the designs for the corresponding wavelengths. The TDFA employs a commercially available core pumped TDF. The authors note that since EDFAs are able to amplify signals at wavelengths up to 1620 nm only the 1620-1650 nm waveband is yet to be covered [27]. Advances in TDFA technology have continued in the recent years as reliable simulation techniques develop and experience continues to mount. In 2018 Tench et al. published simulation and experimental verification of a multiwatt two-stage TDFA, which uses a shared 1567 nm pump source. The optimal lengths of the TDFs and optimal pump coupling ratio for both TDFA stages have been calculated by developing an accurate TDFA model together with accurate measurements of TDF parameters. The achieved small signal gain of up to 60.4 dB and noise figure as low as 3.2 dB highlight the importance of accurate simulation for amplifier optimization. A commercial core pumped TDF was used as a gain medium [7]. Amplifiers of similar make are now commercially available. One of the most recent developments in the field of TDFA research is the use of new fiber doping compositions aimed at “bridging the gap” between TDFAs and EDFAs. In 2019 Chen et al. presented a TDFA based on a germanium/thulium (Ge/Tm) co-doped silica fiber. The Ge/Tm doped fiber shows an intrinsic, blue-shifted absorption/emission cross-section compared to the standard aluminum/thulium co-doped fibers, which greatly improves gain at shorter wavelengths and allows for a gain extension further towards 1600 nm. The blue shift reduces the required inversion for gain below 1650 nm to >60 % which is a great improvement compared to >80 % required for aluminum/thulium doped fibers. The presented amplifier operated in the 1628-1655 nm waveband with maximum small signal gain of 18.7 dB and noise figure as low as 4.4 dB at 1655 nm. The authors noted that overall

optical efficiency is low at $\sim 13.9\%$ but could be improved by further optimizing the dopant composition of the fiber. The core pumped TDF used was manufactured in-house using the MCVD method and solution doping technique [28]. The TDFAs mentioned so far are based on core pumped optical fibers but many EDFAs today employ cladding pumping to make use of cost-efficient multi-mode LDs. A dual wavelength pumped cladding-pumped S-band TDFA was studied in 2007 by Peterka et al. paving the way for further research [29]. Recent research has also produced high power cladding pumped TDFLs [30] but no telecom applications of cladding pumped TDFA are known to the author.

3 Preparation of a depressed-cladding optical fiber

3.1 Background

Depressed-cladding optical fibers have a distinct “W” shape of refractive index profile, which can be engineered to modify the effective refractive index of propagating light to achieve interesting effects. One of these effects has been exploited in optical telecommunication links for dispersion compensation, where a length of dispersion compensating fiber is used to match the dispersion of the whole optical link with the opposite sign resulting in net-zero dispersion. The fibers used for this purpose have a known side effect of rapidly increasing propagation loss at longer wavelengths. The light at longer wavelengths is less well confined to the core, causing it to increasingly propagate through the outer cladding. At some point the effective refractive index of the propagating light decreases below the refractive index of the outer cladding and the light starts to radiate outwards. The depressed-cladding fibers thus have a fundamental mode cutoff, which can be exploited and used as a tunable high pass filter. The tuning is done by bending the fiber, which modifies the refractive index profile of the fiber and consequently the propagation constants. The use of depressed-cladding optical fibers for suppression of ASE has been examined closely for use in S-band EDFAs. Both theoretical analysis and experimental results were presented, showing the viability of these fibers [31, 32].

3.2 Simulation

The refractive index profile of a step-index depressed-cladding fiber generally has four degrees of freedom, those being the refractive index differences between the core and inner cladding Δn and between the inner cladding and the outer cladding Δn_{dep} , the core radius r , and the width of the inner cladding w_{dep} . The fiber outer cladding and core diameter are usually selected to match the passive fiber used in the final application to simplify splicing and minimize splice losses. The refractive index of the outer cladding is, in this case, fixed to the value of pure SiO_2 . The technology used to manufacture the fiber puts

an explicit restriction on the minimum value of Δn_{dep} and an implicit restriction on the maximum value of Δn . To reduce the number of degrees of freedom, it was decided to use an existing core with a given r and Δn , leaving only w_{dep} and Δn_{dep} to be optimized. The optimization was carried out in two major steps. First, propagation constants for straight fibers with various combinations of w_{dep} and Δn_{dep} (parameters) were calculated using a mode solver capable of accepting an arbitrary, radially symmetric refractive index profile as an input [33]. A super-Gaussian approximation of the step-index profile was used to improve accuracy, refer to Figure 1, left for visual reference. The combinations of parameters with the most promising calculated propagation constants were then selected for the second step. In the second step, the losses in the fiber due to bending were calculated at selected wavelengths using a freely available BPM (Beam Propagation Method) toolkit for MATLAB. This toolkit allows to simulate propagation of light through a structure with an arbitrary 3D refractive index profile [34]. The radially symmetric profile used in the first step was first sampled onto a uniform 2D grid, representing the cross-section of the fiber, which was then modified using conformal mapping to model fiber bending. The fiber was considered longitudinally homogeneous with constant bend radius and no twist. The wavelength dependent loss was determined by simulating the coupling of light from a standard single-mode fiber (SMF28) to the depressed-cladding fiber. The beam had a transverse distribution of the fundamental mode of the SMF28 fiber at given wavelength and was normalized to unit intensity at the start of the simulation. Then BPM simulation was then carried out for a 1 m long, coiled depressed-cladding fiber. Lastly, the total intensity of the guided light was compared at several points, with the total intensity launched at the start of the simulation. This way not only the bend loss but also the splice loss of the simulated fiber could be determined. The best combination of parameters was then chosen based on the criteria of high attenuation at long wavelengths and low attenuation at short wavelengths both for a bend radius of a few cm, refer to Figure 1, right for a simulation result example. The splice loss was also taken into account, represented in Figure 1, right by the initial decrease in remaining power from the initial value.

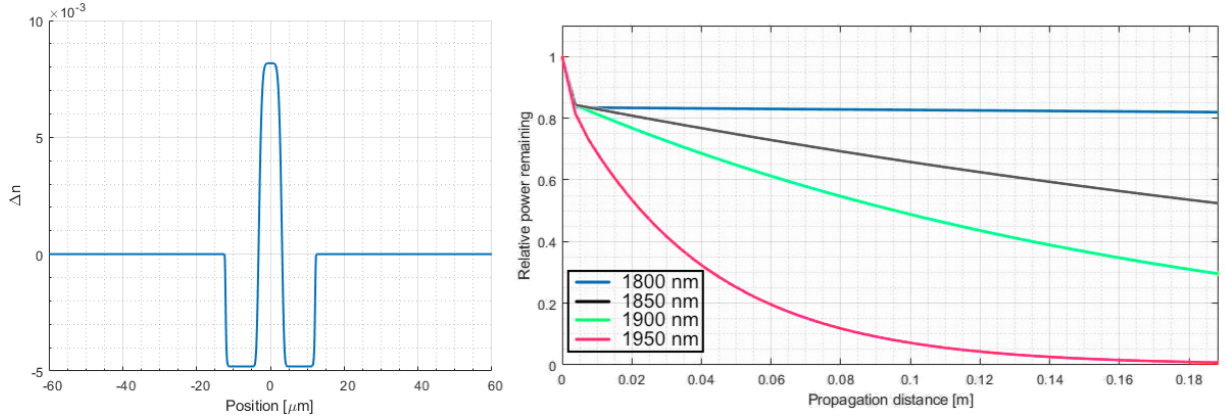


Figure 1: Simulation of depressed-cladding fiber; Left: 1D refractive index profile model; Right: calculated fiber losses for one loop with 3 cm radius at several wavelengths.

3.3 Fiber manufacturing

The fiber preform was manufactured using the MCVD and nanoparticle doping methods with targeted Tm^{3+} doping concentration of ~ 1700 ppm. A refractive index profile measurement was performed, and the data compared to target parameters. The core refractive index of the preform was slightly higher than targeted, and the preform had to be re-sleeved to decrease the r and w_{dep} of the drawn fiber, named SG1797. The final overall length of the SG1797 TDF drawn, was ~ 400 m. Both ends of the fiber were measured to determine the refractive index profiles and doping concentration. The refractive index profile measurements were performed using the IFA-100 optical fiber analyzer, the measured profiles are presented in Figure 2. It was found that the fiber ends differ in both Tm^{3+} doping concentration and, to a smaller extent, refractive index profile. While this inhomogeneity is undesirable for production standard fibers, it presented us with an extra opportunity to experiment with a larger variety of samples. The ends of the fiber will be referred to as two different fibers named SG1797-43 and SG1797-443.

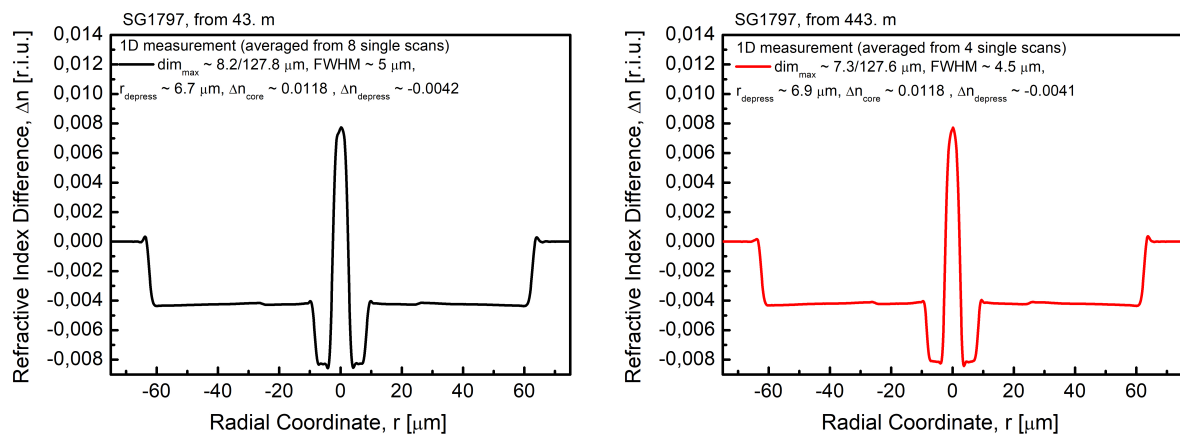


Figure 2: Measured refractive index profiles; Left: SG1797-43; Right: SG1797-443.

4 Amplifier characterization methods

The fundamental function of an amplifier is to amplify an optical signal, a characteristic quantified by optical gain. In addition to the desired optical gain, undesired optical power fluctuations are also added onto the signal, a characteristic quantified most often by noise figure (NF). Both of these quantities are commonly used in literature and by manufactures to describe the performance of amplifiers over a specific intended operating waveband, most commonly quantified as gain bandwidth. The goal of this section is to introduce and summarize the most common and useful techniques used to determine the gain and NF of optical amplifiers.

4.1 Gain

In general, optical gain is a function of both wavelength and signal optical power. For a homogeneously broadened system it stands:

$$G(\lambda) = \frac{G_0(\lambda)}{1 + \sum_k P(\lambda_k)/P_{sat}(\lambda_k)}, \quad (1)$$

where $G_0(\lambda)$ is the small-signal optical gain at wavelength λ , $P(\lambda_k)$ is the optical power, and $P_{sat}(\lambda_k)$ is the saturation power at wavelength λ_k . Gain can be measured by either an optical power meter (PM), an optical spectrum analyzer (OSA) or even an electrical spectrum analyzer. The signal source must be able to cover the whole bandwidth of the amplifier, signal power must be calibrated and varied to accurately measure the saturation effect and a way to filter out the ASE noise, which may impact the accuracy of gain measurements, must be available. Typically, a tunable laser source (TLS) in combination with a variable optical attenuator (VOA) are used to provide signal seed at varying wavelength and optical power. Then a combination of a narrowband optical filter and a PM can be used to measure gain. Note that by using an OSA the requirement for narrowband filtering is removed, which becomes a significant advantage, especially in cases, where exotic wavelengths are used. A quality OSA with high dynamic range can reliably distinguish between ASE and signal power, which provides a powerful tool to measure not only amplifier gain

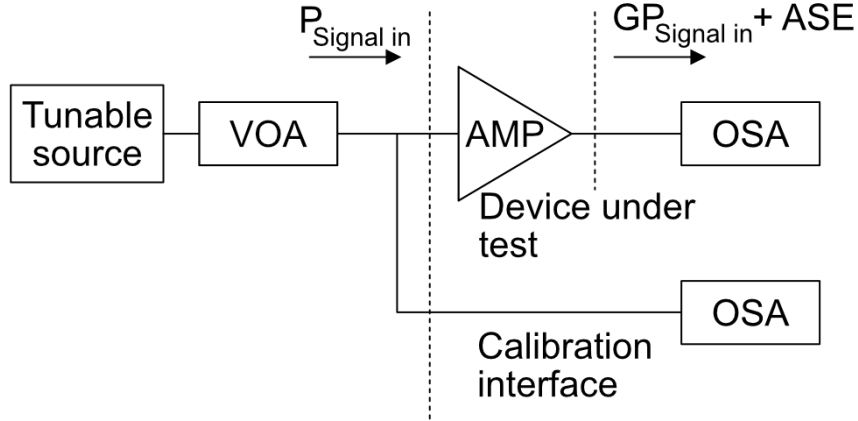


Figure 3: Block diagram of amplifier gain measurement using an OSA; AMP: Amplifier.

but also NF from optical spectra alone as will be discussed later. The block diagram of gain measurement is shown in Figure 3. Note that while the OSA can be exchanged for a PM with a narrowband filter, in cases where the signal optical power is low, and ASE optical power is high a large error to gain measurement will be made. The gain measurement is conducted in the following way: First, $P_{Signal\ in}$ is measured with the amplifier bypassed (Calibration interface), then the OSA and amplifier inputs are switched, and the amplified signal is measured (Device under test). Ideally, an optical switch with no attenuation or multiple OSAs would be used to switch between or simultaneously measure the calibration interface and the device under test. Practically, only a single OSA is used, and the input switched using an optical switch with known characteristics, which need to be accounted for. Note that optical switches for exotic wavelengths may not be available and switching must thus be made manually, which can introduce large error if not done carefully. An example of amplified signal spectra is shown in Figure 4. $P_{Signal\ in}$ is measured through the calibration interface, $P_{Signal\ out}$ and $P_{Noise\ out}$ are measured from the device under test. Note that $P_{Noise\ out}$ is usually hidden under the signal and is thus usually obtained through interpolation as will be further discussed in the NF measurement section. After obtaining the necessary optical power measurements the gain can be easily calculated from the

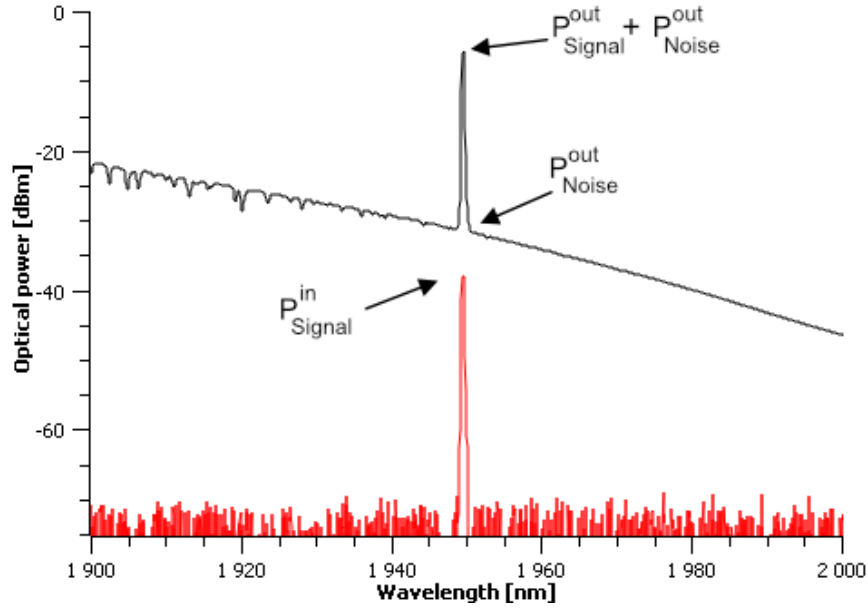


Figure 4: Amplifier output optical power measured using an OSA.

following equation:

$$Gain = 10 \log_{10} \left(\frac{(P_{Signal\ out} + P_{Noise\ out}) - P_{Noise\ out}}{P_{Signal\ in}} \right) \quad (2)$$

Gain being traditionally quantified in dB units [35].

4.2 Noise Figure

Undesired optical power fluctuations added onto the signal by the amplifier, noise essentially, can lead to poor signal reception in analog communications or high bit-error rates in digital communication systems. The concept of NF is commonly used in context of electronic amplifiers but can also be successfully applied to optical amplifiers. It should be noted that not all definitions applied in literature are the same. Different methods of NF measurement can be used depending on the context. In simple cases, for example when a cascade of amplifiers contributes to accumulation of ASE noise, optical measurement methods are usually used. In case the complete NF is required, optoelectronic methods, where the signal is converted from optical to electrical by a photodetector and the electrical signal and accompanying noise are then analyzed using standard electrical methods,

are used. The model examined here and used throughout the thesis is consistent with international standards and is in use by the major test instruments and optical amplifier equipment manufacturers. Both optical and optoelectronic methods are applicable to said model.

4.2.1 Intensity noise

One of the most significant sources of transmission impairment in intensity-modulated communication systems is intensity noise. An optical amplifier can significantly contribute to intensity noise degradation, potentially worsening the signal-to-noise ratio (SNR) of intensity keyed signals to the point of unreadability. An example of SNR degradation is depicted in Figure 5.

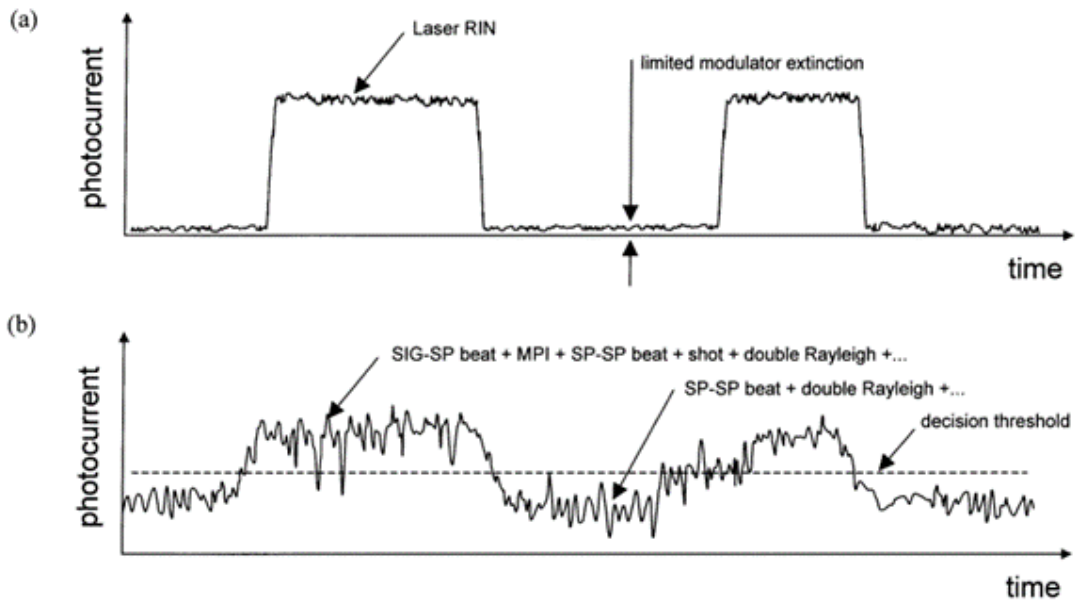


Figure 5: Signal degradation due to amplifier produced noise; a) Transmitter output with SNR as limited by laser relative intensity noise (RIN); b) Received signal corrupted by beat, multipath interference and shot noise. Reproduced with permission from [36].

The transmitter has a good SNR limited mainly by shot noise of the transmitter laser. The progress of the signal through sections of transmission fiber and optical amplifiers reduces

the SNR and increases errors generated by decision circuits that determine whether a logical “1” or “0” was received. Intensity noise contributions include:

- Signal-spontaneous (sig-sp) beating
- Spontaneous-spontaneous (sp-sp) beating
- Amplified double-Rayleigh backscatter
- Multipath interference (MPI)
- Shot noise due to signal, ASE and remnant pump light.

The contributions of various sources to intensity noise are indicated in Figure 5b. The sig-sp beating originates from the mixing or beating of the coherent signal with the incoherent ASE in the same polarization. The sp-sp beat noise is caused by beating of copolarized spectral components of ASE. Rayleigh backscatter is caused by the intrinsic molecular level variations of the refractive index of glass which causes reflections and can contribute significantly to noise in high gain amplifiers. MPI noise arises from the conversion of phase or frequency noise of the signal to intensity noise. The various components and connectors constituting the amplifier can cause internal reflections which then convert the signal phase and frequency fluctuations into intensity noise in a manner similar to a frequency discriminator. Optical reflections may also lead to the enhancement of ASE generation in the amplifier. The main takeaway from this section should be the importance of eliminating internal reflections inside the amplifier as this can lead to excessive generation of MPI and ASE related noise. The elimination of internal reflections is also one of the only factors that can be easily achieved.

4.2.2 Noise figure definition

The NF definition defined in this section covers all the different contributions to noise described in the previous section. The definition is based on a general description of SNR degradation of intensity modulated signals and is valid for all types of intensity noise.

First, the SNR of the input and output signal must be determined. A signal source for the purposes of amplifier characterization should generally be shot noise limited. This means that any excess noise is removed, which is achievable most readily by attenuation. Increasing attenuation in the excess noise regime decreases the noise which converges to pure shot noise. This means that even a relatively noisy signal source can become shot noise limited with sufficient attenuation. All signal sources in this work forward are assumed to be shot noise limited unless stated otherwise. For the input SNR measured by an ideal receiver with unity quantum efficiency, negligible thermal noise, and a noise bandwidth of 1 Hz it stands:

$$SNR_{in} = \frac{P_{in}}{2h\nu} , \quad (3)$$

where P_{in} is the measured power of the signal source and $h\nu$ is the photon energy. The output SNR measured using the same ideal receiver can be obtained from:

$$SNR_{out} = \frac{G^2 P_{in}^2}{S_e(\nu, f) + S_{shot}} , \quad (4)$$

where G is the amplifier gain in linear units, S_e the excess noise spectral density and S_{shot} the shot noise spectral density. Note that S_e generally depends both on the optical frequency ν and baseband frequency f . The degradation of SNR can be then expressed in terms of the noise factor F as a ratio of the input and output SNR:

$$F(\nu, f) = \frac{SNR_{in}}{SNR_{out}} \quad (5)$$

Note the general dependance of the noise factor on baseband frequency is present due to the same dependance of SNR_{out} but is only obtainable using optoelectrical and electrical methods. The measurement of noise factor in the fiberoptic telecommunication industry is a special case where most sources of noise are ignored except for sig-sp beat noise and the optical method is overwhelmingly used. The resulting optical noise factor can be obtained by setting:

$$S_e = S_{sig-sp} = 4\rho_{ASE}GP_{in} \quad (6)$$

$$S_{shot} = 2h\nu GP_{in} , \quad (7)$$

where ρ_{ASE} is the ASE spectral density in the same polarization as the input and amplified signal. We then obtain:

$$F = F_{sig-sp} + F_{shot} \quad (8a)$$

$$F = \frac{2\rho_{ASE}}{Gh\nu} + \frac{1}{G} \quad (8b)$$

The NF is then defined as follows:

$$NF = 10\log_{10}(F) \quad (9)$$

NF is thus expressed in the units of dB. NF can be used to quantify the impact on SNR of not only the whole amplifier but individual components the signal passes through as well. This thus provides a useful tool to evaluate the noise performance of various components of optical telecommunication networks. The usefulness of this tool depends heavily on the correction of non-idealities in the measurement setup as is evident from the various assumptions made during the determination of a practical NF formula. Indeed, comparison between different setups becomes difficult if the individual test setups behave differently in different laboratories and their characteristics cannot be separated from that of the amplifiers. Note that the IEC, an organization responsible for the definition of various technical standards, defines the noise factor as only the first term in Equation 8b.

4.2.3 Noise factor of an optical cascade

In a cascade of optical components and amplifiers the gain evolves in a multiplicative fashion and the noise factor evolves in multiplicative and additive fashion. Having a method to express this cumulative effect in terms of an overall NF of an optical cascade is useful in prediction of effects the various components have on the overall NF. Each stage of a cascade adds noise to the signal and simultaneously amplifies noise from the previous stages. The total sig-sp noise factor of a cascade with N stages is given by:

$$F_{sig-sp}^c = F_{sig-sp,1} + \frac{F_{sig-sp,2}}{G_1} + \frac{F_{sig-sp,3}}{G_1 G_2} + \dots + \frac{F_{sig-sp,N}}{G_1 \dots G_{N-1}}, \quad (10)$$

where $F_{sig-sp,N}$ is the noise factor of the Nth stage. Once the sig-sp noise factor is calculated the shot noise factor inclusion is straight forward:

$$F_{sig-sp,shot}^c = F_{sig-sp}^c + \frac{1}{G_1 \cdots G_N} \quad (11)$$

Note that a passive component is characterized by loss L to which the corresponding gain G is set.

4.2.4 The optical method

The NF measurement through optical techniques is carried out using an OSA to measure the spectral density of ASE, from which the noise factor is determined according to Equation 8b. It is important to refer to the noise performance of an amplifier while clearly having defined the corresponding set of input and output terminals. Input power is defined by the IEC as the power exiting the input connector, or cleaved fiber prior to the fusion splice connection. It is of great importance to keep the input coupling loss to minimum as it can have a dramatic effect on the measured NF. This effect can be determined using the cascade formula from Equation 11. This contribution must be either corrected or accounted for to provide accurate measurements. The easiest way to reduce or eliminate the input power attenuation is to use fusion spliced connections. The situation can be paraphrased in relation to the output signal port. Since the general requirements and parameters for accurate measurements have been determined and discussed, the method of how to obtain said parameters will be discussed next. As a reminder the parameters to be measured are:

- The ASE spectral density: ASE in the signal polarization, at the signal wavelength ρ_{ASE}
- The signal wavelength: optical frequency ν
- The amplifier gain: G

The ASE spectral density in the signal polarization can be easily measured using an OSA, while the ‘same polarization as the signal’ requirement is usually satisfied by dividing the

total spectral density by a factor of 2, except for cases where polarization hole burning is of concern. The measurement of gain has been discussed in the preceding sections and the signal wavelength can be determined in a variety of ways. While the optical method of measurement is straight forward when ideal signal sources and detectors are available, that isn't always the case. A number of improvements to the optical method have been developed to account for some of these non-idealities, including:

- Source subtraction
- Time domain extinction
- Polarization extinction
- Signal substitution

The amplifier gain is measured at signal wavelengths in all measurements and the amplifier generated ASE is measured at the same wavelengths, or at adjacent wavelengths and obtained via interpolation. The interpolation is carried out between two points each adjacent to one side of the signal peak. Note that accurate information about the noise bandwidth of the used OSA is required and that it is not necessarily equal to the resolution bandwidth. The noise bandwidth can be accurately calculated as the FWHM of the detected signal peak as long as the resolution isn't too high (i.e. <0.05 nm) [37].

4.2.5 Source subtraction technique

In case a non-shot-noise-limited signal source is used, and source spontaneous emission (SSE) is encountered, the source subtraction technique can help in improving the measurement accuracy. First, the source SSE is characterized with the amplifier bypassed. Assuming the SSE is time invariant it can, in principle, be subtracted from the amplifier ASE. To accommodate the correction, Equation 8b is modified as follows:

$$F = \frac{2\rho_{total}}{Gh\nu} + \frac{1}{G} - \frac{2\rho_{SSE}}{h\nu}, \quad (12)$$

where ρ_{total} and ρ_{SSE} are the total spontaneous emission from the amplifier including the SSE and SSE spectral densities respectively. The technique is illustrated in Figure 6.

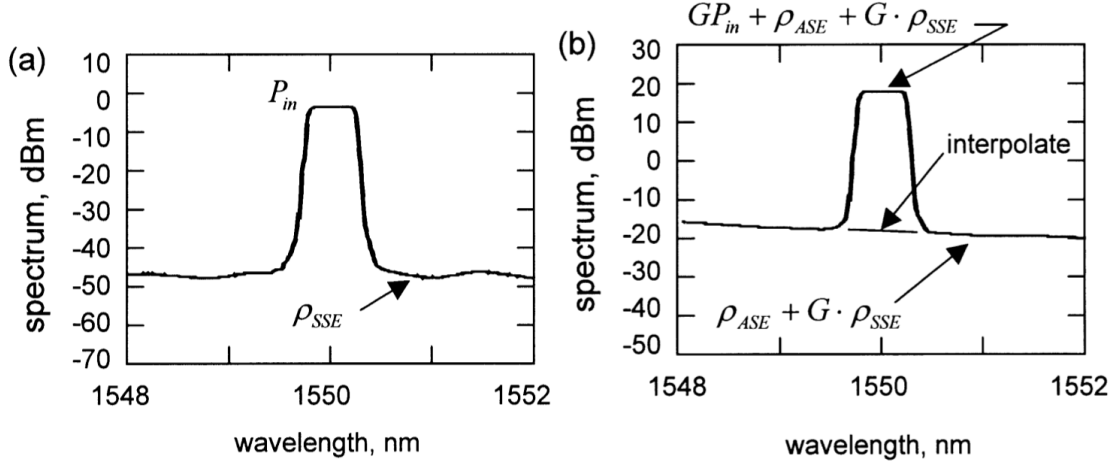


Figure 6: Optical spectra for source subtraction method of noise figure measurement; a) incident signal and SSE; b) output spectrum. Reproduced with permission from [36].

4.2.6 Polarization extinction technique

This technique assumes a fixed or known relationship between the magnitude of the generated ASE in orthogonal polarizations. Therefore, if the ASE is measured in one polarization, the ASE in the signal polarization becomes known. A polarization controller (PC) and a polarizer are inserted after the amplifier and the PC is set such that the signal polarization is orthogonal to the preferred transmission axis of the polarizer to measure the ASE. These conditions ensure that the signal, the amplified SSE and one-half of the ASE do not reach the OSA. The OSA thus measures only the ASE orthogonal to the signal. The noise factor is then calculated from Equation 8b, assuming equal ASE densities in both polarizations. The signal rejection may not be complete, nevertheless the accuracy of the measurement will be higher. Interpolation can be used, as discussed previously, to remove remaining signal from the ASE spectra. The gain is measured as described in previous sections, without the PC and polarizer. A major advantage of this technique is the reduction in required optical rejection ratio of the OSA. The limited wavelength selectivity limits the

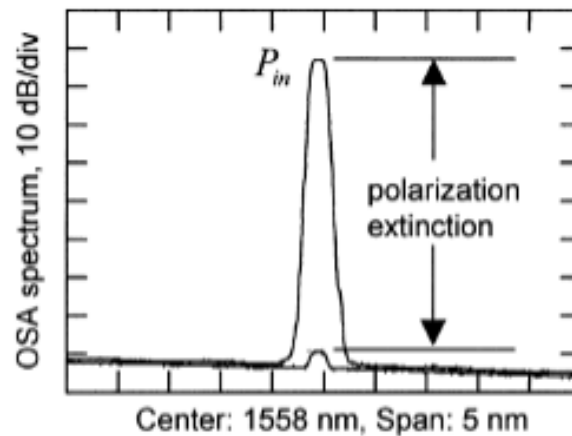


Figure 7: Input signal and laser spontaneous emission rejection using polarization extinction. Reproduced with permission from [36].

ability of an OSA to measure weak signals at very close wavelengths to a strong signal. By eliminating the signal, it becomes possible to perform ASE measurements much closer to the signal wavelength. An illustration of the discussed effects is provided in Figure 7.

5 SG1797 TDF attenuation measurement

The attenuation measurement of both SG1797-43 and SG1797-443 was carried out using a spectrally broad light source with an SMF28 patch cord inserted between the measurement points to provide a reference attenuation value. First a short section (~ 11 cm) of straight fiber under test (FUT), where excess loss is more easily distinguishable from the Tm^{3+} absorption band, was measured using a fiber coupled halogen lightbulb to determine Tm^{3+} doping concentration. The spectra of transmitted light were captured using a Thorlabs OSA203C OSA. The result of this measurement is presented in Figure 8, left. Then, to measure the bend loss more accurately, a longer section (~ 1 m) of FUT was used. The FUT was spliced to two SMF28 pigtails to provide connectivity. The FUT was then coiled with varying radii and number of loops to verify the effect of various coiling conditions, some more complex bending shapes were also examined. Absorption is too strong near the Tm^{3+} absorption band and thus requires higher light intensity to illuminate the spectral features in this area. A thulium-doped fiber optic amplified spontaneous emission (Tm:ASE) source [38] was used as a signal source in this range. Attenuation of the ~ 1 m long FUT, again referenced to an SMF28 patchcord, subsequently used as a reference for the bending experiments is presented in Figure 8, right. The Thorlabs OSA203C was used to capture the transmitted spectra. The observed spectral features hint at slight differences between SG1797-43 and SG1797-443 both in Tm^{3+} doping concentration and transmission characteristics. This fact is further proven by the coiling experiments, the results of which are presented in Figure 9. These results were later used in selection of suitable fiber and fiber length of the tunable laser sources and amplifiers. A general graphical description of the FUT bend shapes used in attenuation measurements is displayed in Figure 10.

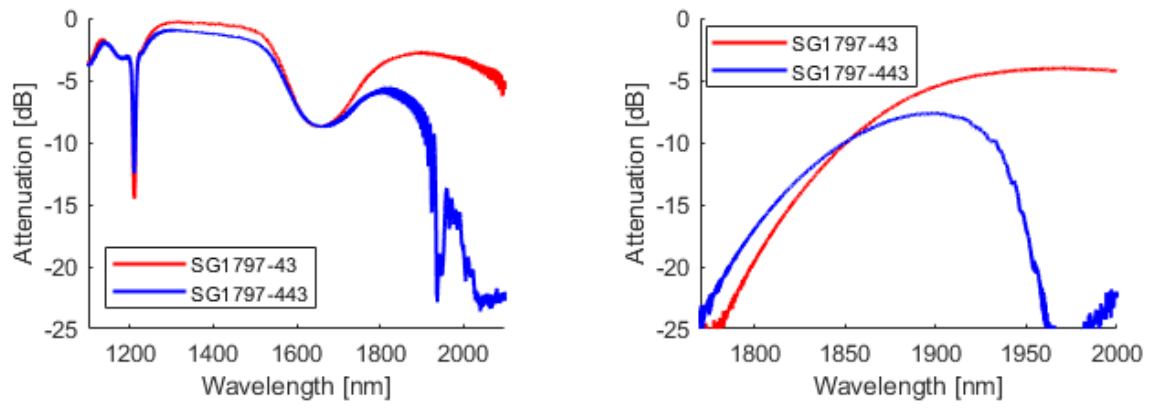


Figure 8: Attenuation measurements of SG1797 fiber; Left: measurement of ~ 11 cm of straight FUT to determine Tm^{3+} doping concentration; Right: Measurement of ~ 1 m long FUT to determine excess loss near the absorption band.

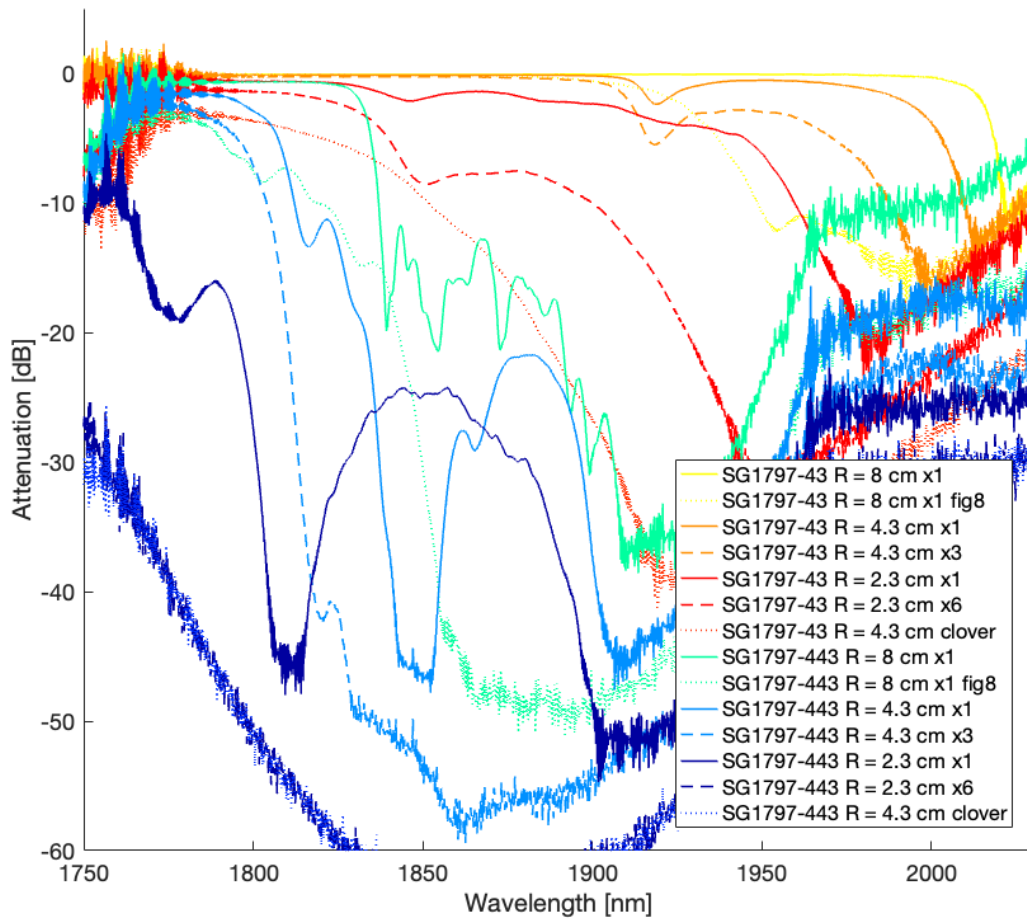


Figure 9: Detail of FUT bend loss near the Tm^{3+} absorption band; clover: the whole FUT is coiled with $R = 4.3$ cm and then deformed at four points distributed in a cross pattern with each attachment point being 3.25 cm from the center; fig8: one loop of fiber with $R = 8$ cm is made and then twisted into a symmetrical figure 8 shape.

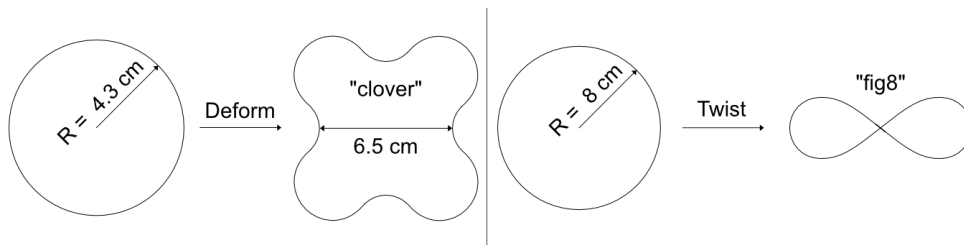


Figure 10: FUT bend shapes.

6 TTDFL experimental setup

One of the best ways to measure signal gain and NF of fiber optic amplifiers over a wide spectral range is to use a tunable laser source as signal seed. Such a source must be tunable over the whole spectral bandwidth of the amplifier under test and have sufficient SNR as well as output power. It is difficult to satisfy all the requirements simultaneously using a single, static, setup. The obvious solution is then to have multiple setups or setups which can be easily modified to deliver satisfactory performance at any given time. For the 1650-2050 nm spectral range, two modifiable setups were developed, named TTDFL-S and TTDFL-L (Tunable Thulium-Doped Fiber Laser). Both are core pumped by an in-house built EDFL, which provides up to 1.8 W of continuous power at 1565 nm. A polarization independent (PI) optical isolator was placed between the EDFL pump and the TTDFL to protect the pump from any light from the TTDFL, which could cause unexpected behavior of the EDFL.

6.1 TTDFL-S experimental setup

The TTDFL-S is designed specifically for the 1650-1800 nm range. A wavelength division multiplexer (WDM) which has low insertion loss at 1650 nm is used to couple the pump to the active fiber. Its insertion loss increases rapidly around 1800 nm, which also helps suppress parasitic lasing at longer wavelengths. A Richardson Gratings 600 grooves/mm ruled reflection grating with a blaze wavelength of 1850 nm was used as a wavelength selective element. Used as the gain medium, 1.2 m of the SG1797-433 fiber was placed on a flexible board in a bent pattern. The losses in the resonator can be influenced by bending the flexible board to a “U” shape, which serves to suppress longer wavelength ASE and prevent parasitic lasing, when the laser is tuned to short wavelengths. The setup uses a broadband 50:50 fused optical coupler optimized for 1550 nm with a fiber PC as a fiber loop mirror and output coupler. This type of mirror has adjustable reflectance, which can be used to optimize performance of the TTDFL. The setup is schematically depicted in Figure 11. Since the length of the TDF is quite short, larger than negligible amounts of

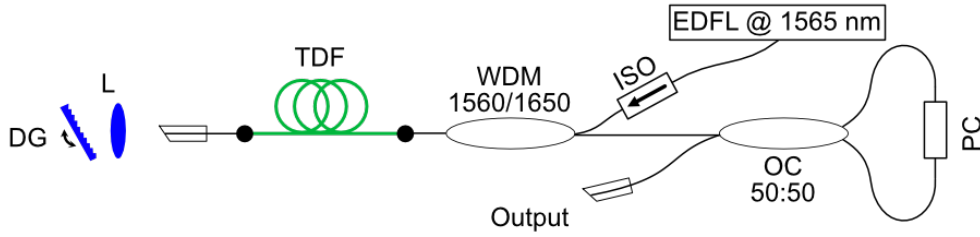


Figure 11: TTDFL-S experimental setup; DG: diffraction grating; L: aspheric lens; OC: output coupler.

unabsorbed pump power exit the TDF at the tuning side of the resonator. The diffraction grating serves as a natural residual pump dumping device by reflecting the remaining pump light at an angle to a beam dump area.

6.2 TTDFL-L experimental setup

The TTDFL-L is designed specifically for the 1800-2050 nm range. The pump power was coupled into the active fiber by a 1560/1950 nm WDM. As a gain medium, 2 m of core-pumped highly doped (~ 3200 ppm Tm^{3+} , 4.5 mol% Al_2O_3 concentrations) TDF, which was prepared in-house using the MCVD method and solution doping method, was used. A Richardson Gratings 600 grooves/mm ruled reflection grating with a blaze wavelength of 1850 nm was used as a wavelength selective element. A perpendicularly polished FC type connector serves as a $\sim 4\%$ mirror as well as the output coupler. The experimental setup used for the TTDFL-L is illustrated schematically in Figure 12.

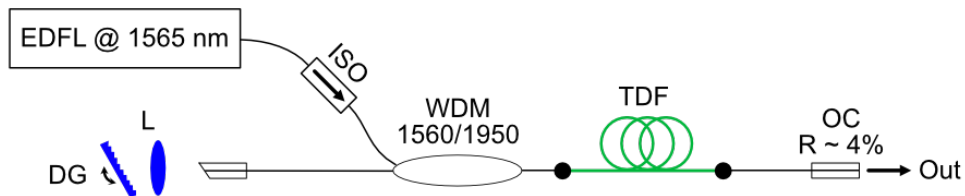


Figure 12: TTDFL-L experimental setup; DG: diffraction grating; L: aspheric lens; OC: output coupler.

The longer length and higher doping of the TDF used in TTDFL-L leads to improved pump absorption compared to TTDFL-S. The residual pump is thus negligible and usually >35 dB lower in intensity than the produced signal.

6.3 TTDFL characterization

The characterization of the TTDFL includes testing the tunability of the laser, measurement of maximum output power across the whole tuning range and investigation of laser operating regime. All necessary measurements can be carried out at the same time using a single measurement setup. The setup consists of a 99:1 spectrally flat fused optical coupler connected to the output of the TTDFL, which first routes most of the signal towards a power detector from the 99% port. The 1% port routes the rest of the signal through a VOA towards a 70:30 spectrally flat optical coupler, which routes 70 % of the signal towards a fast power detector connected to an oscilloscope. The remaining 30 % of the signal is sent to an OSA that displays the current output spectra of the TTDFL. The measurement setup is schematically shown in Figure 13.

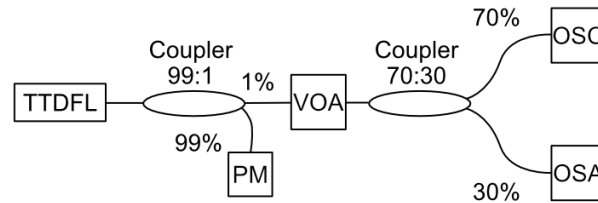


Figure 13: TTDFL characterization scheme; OSC: oscilloscope.

A Thorlabs S148C integrating sphere photodiode power sensor with a PM100D Thorlabs power meter were used to measure the output power of the TTDFL. The spectral characterization was performed using the Thorlabs OSA203C OSA. The SNR of TTDFL-L was later verified using the Yokogawa AQ 6375B OSA, which has a higher optical rejection ratio, during the gain and NF measurements of the TDFA-L. The temporal characteristics of the TTDFL were measured using the Thorlabs PDA10D2 photodiode detector and LeCroy HDO6034 oscilloscope.

7 TDFA experimental setup

Covering the whole spectral region 1650-2050 nm with a single amplifier design would most likely lead to unsatisfactory performance over the whole bandwidth as the Tm^{3+} ions in silica based TDFs exhibit strong three-level behavior in the 1650-1800 nm region and have a relatively small emission cross-section in the 1950-2050 nm region, which both require special attention and contradicting design choices. It has been decided to develop three different amplifier setups, two for the region 1650-1800 nm and another for the 1800-2050 nm spectral region. All three setups employ commercially available optical components, with some of the fused optical components previously developed in collaboration with SQS VláknoVá optika company [39].

The 1650-1800 nm range amplifier, named TDFA-S, employs a novel design which features a depressed-cladding TDF SG1797, the preparation of which has been described in Section 3. Since ASE generation, predominantly occurring on wavelengths longer than those the fiber can guide, is effectively suppressed, a high inversion of population can be maintained. Two TDFA-S setups with different pumping schemes were developed.

7.1 TDFA-S-790 experimental setup

The first setup, named TDFA-S-790, is core pumped by an LD at 790 nm. Core pumping in this case necessitates a single mode LD, which limits the available pump power as single mode LDs currently only reach maximum output power in the order of hundreds of milliwatts. The pump power is coupled to the TDF via a 790/2000 nm WDM. Forward pumping was selected to limit the optical power propagating in the direction of the LD. The input and output ports of the amplifier are protected against undesired reflections by PI optical isolators, which also ensure unidirectional operation of the amplifier. The experimental setup is illustrated in Figure 14. Both SG1797-43 and SG1797-443 were tested with varying bend radii, the attenuation of which was described in Section 5. A standard TDF, named SG1603 (~ 1700 ppm Tm^{3+} , 8 mol% Al_2O_3), was also tested for

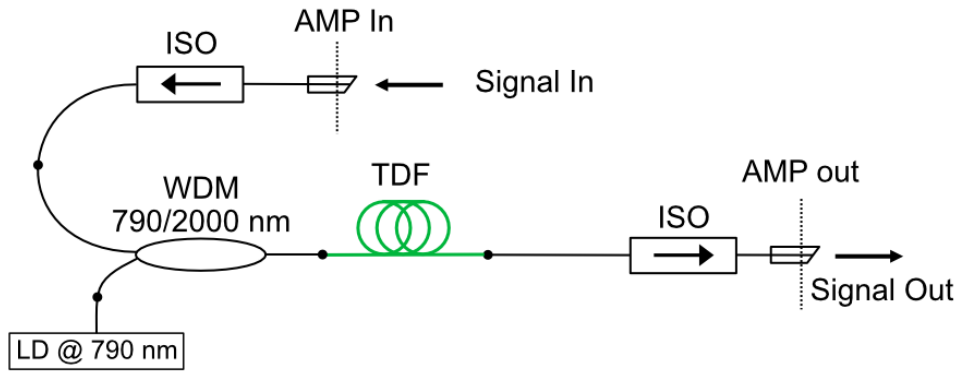


Figure 14: TDFA-S-790 experimental setup; AMP: amplifier; ISO: optical isolator.

comparison. The length of the TDF was calculated using a simplified amplifier model to achieve sufficient inversion at shorter wavelengths. The length was then optimized using the cutback method. The optimized lengths of fiber are 85 cm of SG1797-443, 50 cm of SG1797-43 or 50 cm of SG1603.

7.2 TDFA-S-1565 experimental setup

The second setup, named TDFA-S-1565, is core pumped by an in-house-built EDFL in a ring arrangement emitting at 1565 nm. The maximum available pump power is 3.8 W. The pump power is coupled to the TDF via a 1550/1750 nm WDM, with low insertion loss at both pump and signal wavelengths. The input and output ports of the amplifier are protected against undesired reflections by PI optical isolators and ensure unidirectional operation of the amplifier. The experimental setup is depicted in Figure 15. The intensity of ASE generated at longer wavelengths necessitates the use of the new depressed-cladding fibers which is a consequence of the magnitude more powerful pump compared to the 790 nm LD. The best configuration found employs a 1.5 m long section of tightly wound SG1797-43 fiber in a “figure 8” shape. A rough outline of the “figure 8” fiber bend shape is also depicted in Figure 15. A forward pumping scheme was selected to provide better isolation of the TTDFL from remaining pump power and of the pump laser from amplified signal. Relatively high amounts of unabsorbed pump power enter the measurement setup

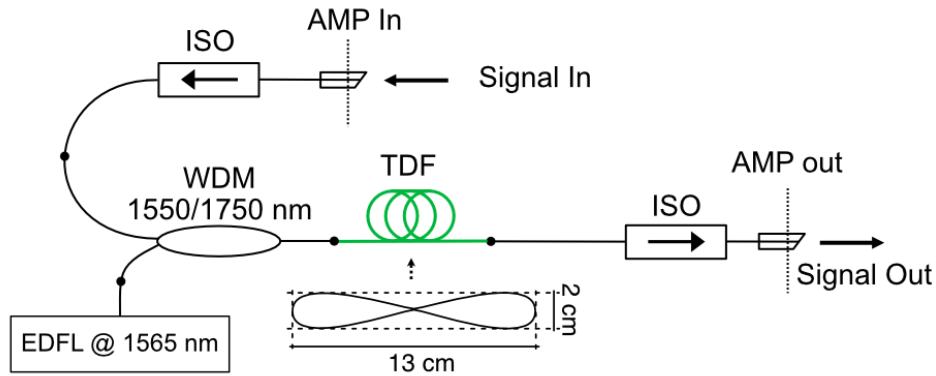


Figure 15: TDFA-S-1565 experimental setup, note the TDF bend shape used in this setup; AMP: amplifier; ISO: optical isolator.

due to the short length of the TDF. It was thus decided to limit the maximum pump power to 1.9 W in most cases.

7.3 TDFA-L experimental setup

The 1800-2050 nm range amplifier, named TDFA-L, operates in a more well-explored spectral range for TDFs and can thus employ a more orthodox design. The previous work done in the scope of the author's bachelors theses yielded a Tm:ASE source for the spectral region 1800-2000 nm with an output power of >130 mW, which can be used as a starting point for the development of the TDFA-L. The Tm:ASE source has a broad emission spectrum of more than 140 nm at the -3 dB level with two local peaks at around 1850 nm and 1950 nm. The width and center of the emission spectrum can be optimized by varying the length of the active fiber or by varying the pump power, thus theoretically allowing for amplifier fine tuning. The experience gained during the development of the Tm:ASE source provided an initial estimate for the length and type of TDF to be used as gain medium. The TDFA-L also shares the same general topology with the Tm:ASE source with several differences. The most significant difference being the removal of a metallic mirror, which served to reflect forward ASE backwards for further amplification, and an addition of an optical isolator for the input signal [38, 40]. Both devices employ

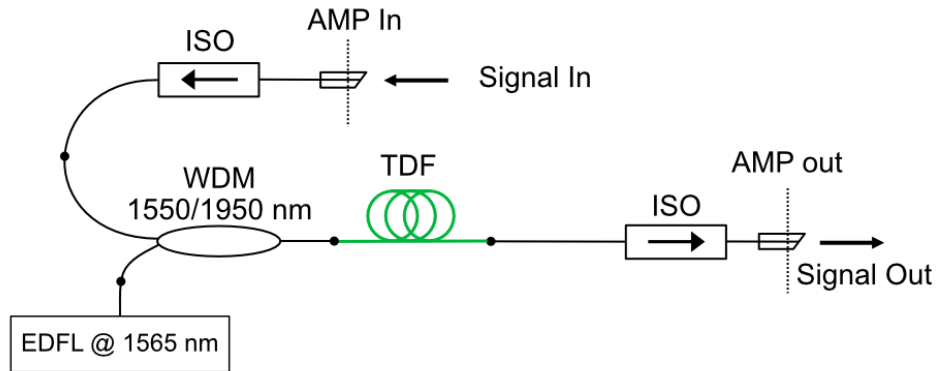


Figure 16: TDFA-L experimental setup; AMP: amplifier; ISO: isolator.

a simple all-fiber geometry utilizing commercially available optical components except for the active fiber, which has been developed and manufactured in-house. An in-house-built EDFL in a ring arrangement emitting at 1565 nm is used as an in-band pumping source with a maximum output power around 2.3 W. The EDFL pump was built and characterized during work on the author's bachelor thesis [41]. The EDFL can be easily modified to serve as an EDFA and utilized as an amplification module elsewhere. The pump is coupled into the active fiber by a 1560/1950 nm WDM. A forward pumping scheme was selected based on better noise performance when amplifying small signals. The input of the amplifier is optically isolated by a PI optical isolator and the output is secured in the same way against back-reflections by an identical isolator. The setup is schematically depicted in Figure 16. The TDF was chosen first based on its mechanical properties such as fiber diameter and numerical aperture to be as similar to an SMF28 fiber as possible to minimize splice losses and avoid other issues related to steep changes in waveguide properties. The selection was further narrowed down by the laser properties of the selected fibers. Based on these criteria two types of TDF, named SG1290 and SG1603, were chosen. The SG1290 TDF was previously used in the Tm:ASE source and was thus an obvious choice, the SG1603 was chosen mainly for its better fluorescent lifetime properties at the relevant energy level. Based on the results presented in [42], 5 m of SG1603 fiber was determined optimal in this application.

7.4 TDFA characterization

The characterization of all three TDFA setups was conducted in a similar manner. First the signal from either TTDFL-S or TTDFL-L was adjusted using a VOA and then split by using a 50:50 coupler. A Thorlabs S148C integrating sphere photodiode power sensor with a PM100D Thorlabs power meter were used to monitor the power at the input of the amplifier using the first port of the coupler. Three general signal input power levels of approximately -20 dBm, -10 dBm and 0 dBm were selected to characterize the TDFA and to evaluate amplification of both small and large signals. The second port of the coupler was connected to the amplifier or bypassed the amplifier in case the signal reference was being measured (recall Figure 3). The VOA and the 50:50 coupler can be omitted if the operation of the TTDFL is stable and providing the correct signal power. A 99:1 optical coupler was inserted after the amplifier or directly after the 50:50 coupler to split the amplified signal or reference signal respectively. The total power of the signal was monitored at the 99% port of the coupler using a Thorlabs S405C thermopile power detector with a PM100D Thorlabs power meter. An OSA was used to capture the signal spectra. The gain and NF characterization was performed using the Thorlabs OSA203C for both TDFA-S setups and the Yokogawa AQ6375B was used for the TDFA-L setup. The block diagram of the measurement setup is shown in Figure 17. The Thorlabs OSA203C was set to low resolution, high sensitivity setting with either single or double pass Hann apodization. A MATLAB script has been developed which automatically detects narrowband peaks and calculates gain and NF based on user defined parameters. The interpolation method was used to determine the ASE noise level, the user must then decide whether the ASE noise level is determined correctly based on a spectral graph. The gain and NF were calculated using the methods described in Sections 4.1 and 4.2. Since the optical rejection ratio of the Thorlabs OSA203C is often insufficient for NF measurement using this method some helpful techniques outlined in Section 4.2. can be used instead. The Yokogawa AQ6375B was set to a resolution of 0.2 nm and the EDFA-NF function was used to calculate gain and NF. Automatic settings were used where possible but for some measurements the fitting

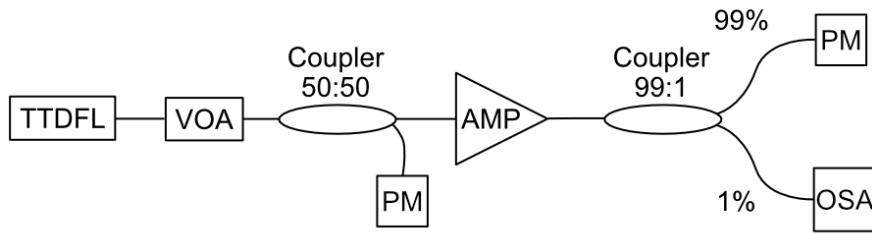


Figure 17: TDFA gain and NF measurement; AMP: amplifier; PM: power meter.

algorithm and related parameters needed to be set manually. These measurements were later verified using the same MATLAB script mentioned earlier. The difference between the methods used for calculation is in determining the equivalent noise bandwidth. The Yokogawa AQ6375B preferably uses factory calibrated equivalent noise bandwidth values stored inside the device, whereas the MATLAB script determines the equivalent noise bandwidth from signal FWHM. The difference between the two is negligible at the 0.2 nm resolution used. Note that the amplifier input and output ports for gain and noise figure measurements are defined at the input isolator input connector and output isolator output connector respectively as noted in the individual amplifier schemas. Spectral and power measurements are corrected for the spectral characteristics in of the 99:1 coupler either in the OSA or later in software.

8 Results and discussion

8.1 TTDFL-S results

The TTDFL-S setup covers wavelengths from 1650 nm to 1800 nm, which meets the goals set for this device. The TDF must be bent accordingly to enable tuning across the whole range. Spectral measurements showing the tunability coverage of this setup and spectral intensities of the output signal are shown in Figure 18, the inset shows the same measurement only at 1650 nm performed using an ANDO AQ6317 OSA with an identical measurement setup. A VOA was used to limit the influence of differences in total output power at different wavelengths so that all peaks appear to have a similar height.

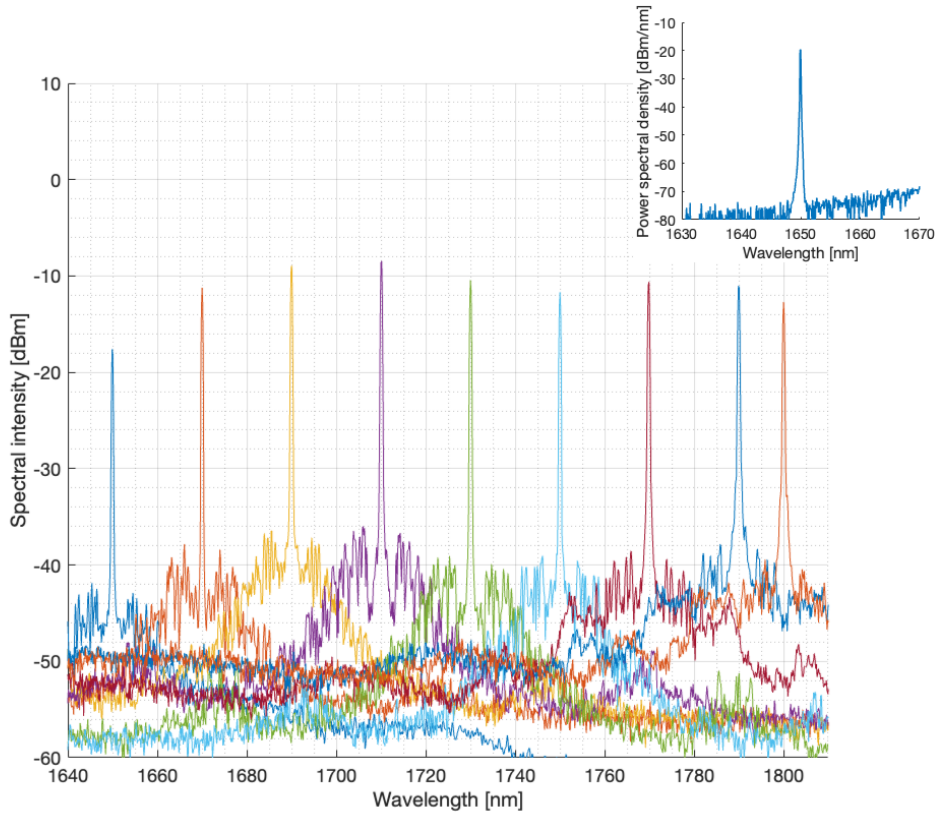


Figure 18: TTDFL-S output spectra at maximum pump power. Inset measured using ANDO AQ6317.

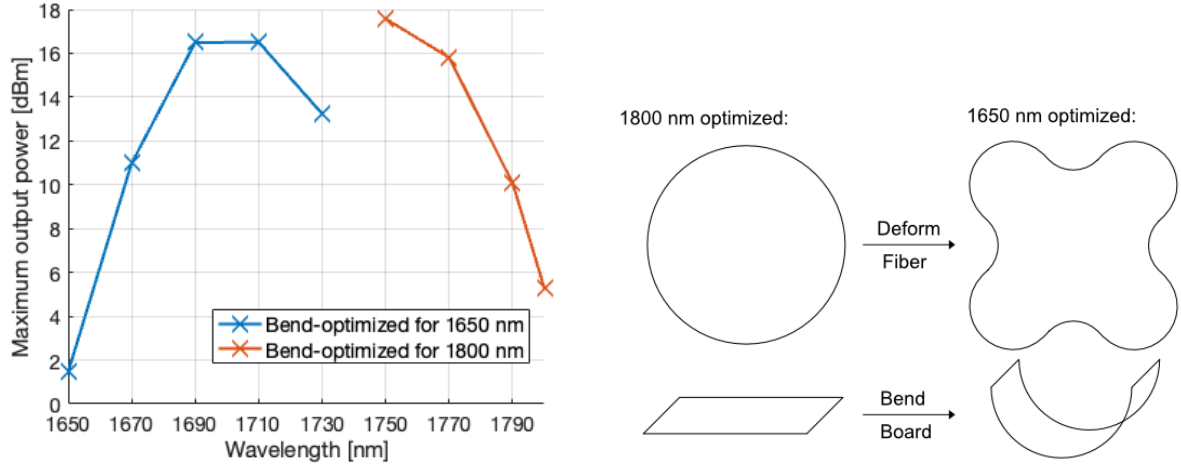


Figure 19: Left: TTDFL-S evolution of maximum output power over the covered range; Right: graphical description of TDF bend optimization.

The SNR discernable from the spectra is sufficient for accurate gain and NF measurements. Visible sidebands appear near the main laser peaks, usually ~ 30 dB lower in intensity than the laser peak. Those sidebands are by and large random and not present on spectra measured using OSAs that employ a monochromator, such as the ANDO AQ6317. It is therefore reasonable to assume that the sidebands are a measurement artifact of the Thorlabs OSA203C OSA, the probable cause being the operating regime of the laser. The maximum output power of the TTDFL-S setup is presented in Figure 19, left. Figure 19, right provides a general graphical description of the TDF bend needed to achieve these results. The setup is sufficiently powerful to satisfy the needs of amplifier characterization, nevertheless the efficiency is somewhat poor, which is mostly caused by large amounts of unabsorbed pump power. The laser operates in free-running mode most of the time, the exception being at laser threshold where distinguishable pulses form. Examples of the free-running regime and pulsing at low power of the TTDFL-S, captured at 1790 nm with maximum pump power and at laser threshold respectively, are displayed in Figure 20. The pulsed regime can be damaging to optical amplifiers so operating the laser near the laser threshold should be avoided.

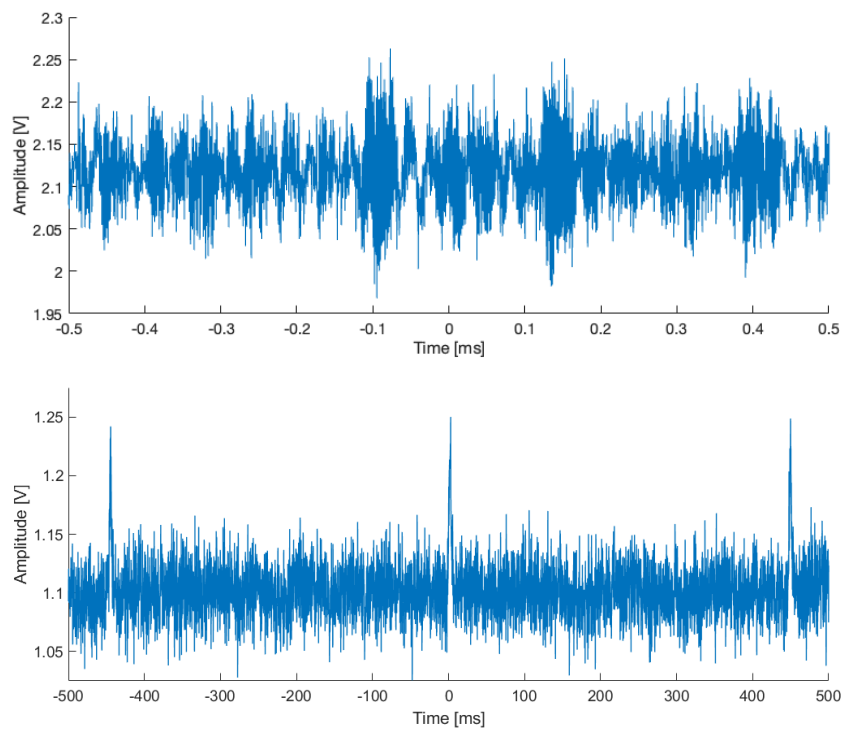


Figure 20: Oscilloscope traces displaying the operating regimes of the TTDFL-S; Top: at maximum pump power; Bottom: at laser threshold.

The TTDFL-S meets all requirements for amplifier characterization specified earlier. A major flaw of this setup is the poor repeatability of TDF bending which is mostly random and not easily parametrized. For now, setting the optimal fiber bend shape and radius requires the laser operator to closely monitor laser performance while manually bending the fiber. The solution to this problem would be to construct a bending mechanism, which would deform the fiber in well-established patterns to allow easy wavelength and performance tuning of the laser. Determining the best shape of this mechanism is a difficult task as experience has shown that the more random the bend pattern is the better ASE suppression is achieved.

8.2 TTDFL-L results

The TTDFL-L setup covers wavelengths from 1810 nm to 2050 nm, which can be further increased by introducing additional resonator loss at longer wavelengths to reach 1800 nm. The tunability was measured only across the 1810-2050 nm range as wavelengths <1810 nm can be easily covered by TTDFL-S. The output spectra for the whole tuning range at maximum pump power are presented in Figure 21, note that the peaks are normalized to actual output power. The 1810 nm peak shows periodic sideband artifacts in this measurement, which are not present when measuring amplifier gain or when the measurement is made using a different OSA. An ASE peak centered at 1870 nm can be observed when the wavelength is set to 2050 nm. It can be lowered by fine tuning the pump power and maximizing reflectivity of the blazed DG. The maximum output power measured over the whole covered range is displayed in Figure 22. The output power of the TTDFL-L setup exceeds the requirements for amplifier characterization purposes. The laser operates in free-running regime most of the time, sometimes transitioning to continuous regime at high power settings. Examples of the free-running nature and continuous nature of the TTDFL-L, captured at 1900 nm at laser threshold and with maximum pump power respectively, are displayed in Figure 23. The TTDFL-L setup overall meets the requirements set for amplifier characterization.

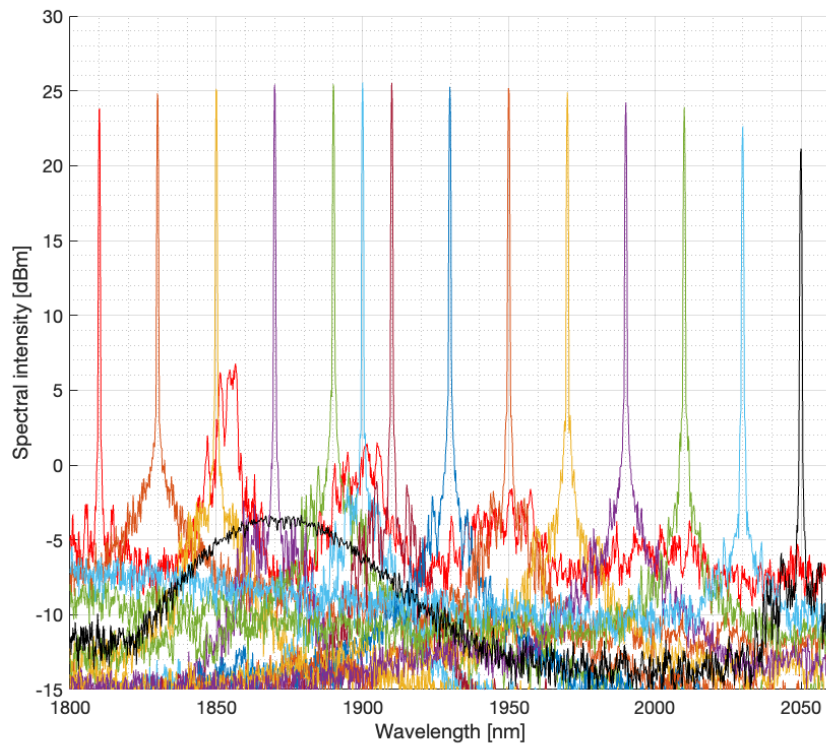


Figure 21: TTDFL-L output spectra at maximum pump power.

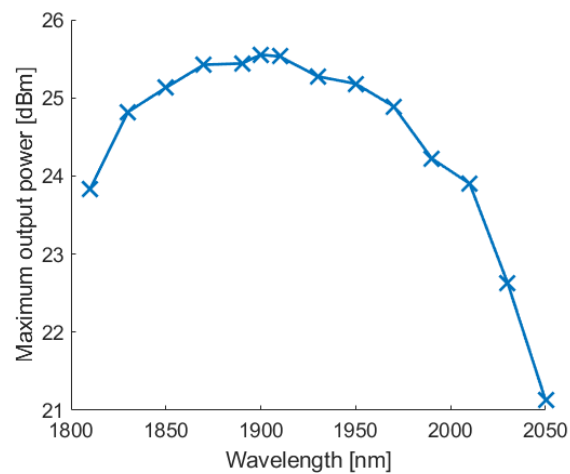


Figure 22: TTDFL-L evolution of maximum output power over the covered range.

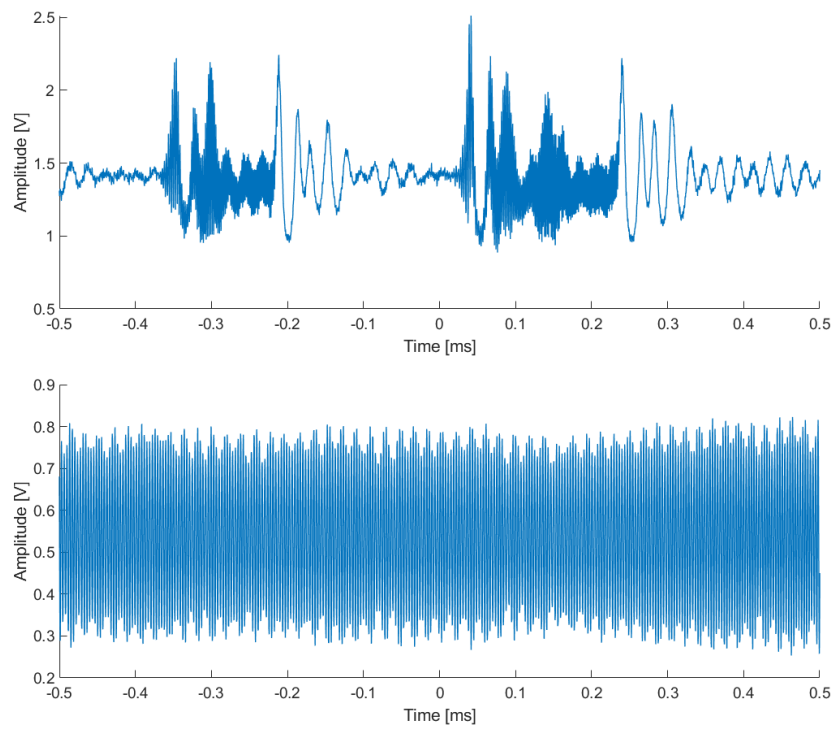


Figure 23: Oscilloscope traces displaying the operating regimes of the TTDFL-L; Top: at laser threshold; Bottom: at maximum pump power.

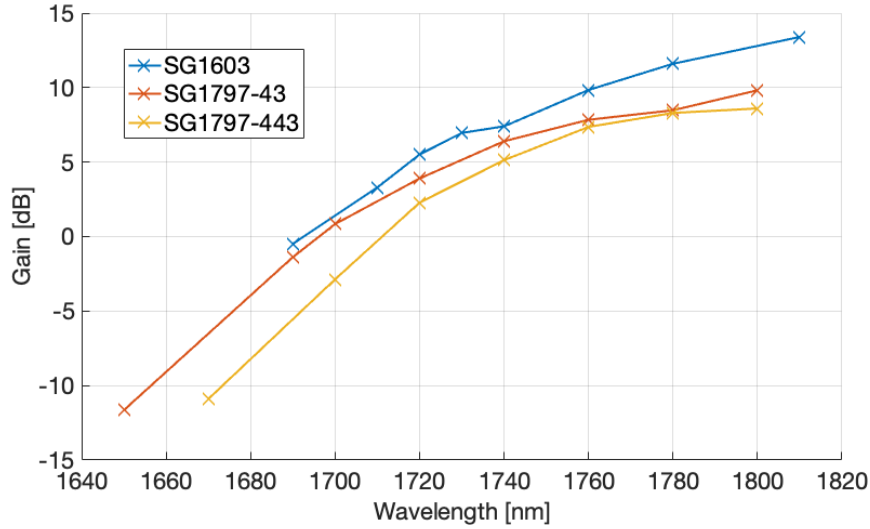


Figure 24: TDFA-S-790 gain.

8.3 TDFA-S-790 results

The TDFA-S-790 setup produced low to negligible gain in the covered range. The gain at wavelengths <1690 nm is negative, meaning the losses induced by the optical components, excess losses in the TDF and absorption outweigh the gain. Gain at selected wavelengths for the SG1603, SG1797-43 and SG1797-443 fibers is displayed in Figure 24. Only a single input signal power setting around -20 dBm is presented as this presents the best-case scenario with higher input signal power reducing the gain and lower input signal power not considered applicable. It is apparent that the standard SG1603 TDF outperforms the new depressed-cladding TDF, which can be attributed to higher splice and intrinsic loss of the new fiber. The effect of ASE suppression is negligible as the relatively low power of the pump LD is unable to produce significant ASE to begin with. Any losses incurred by additional bending of the fiber thus outweigh any gains made by increasing the inversion by ASE suppression. Accounting for the total insertion loss of the optical components (two optical isolators, one WDM) at 1700 nm of 3.7 dB doesn't significantly improve the prospects of this setup.

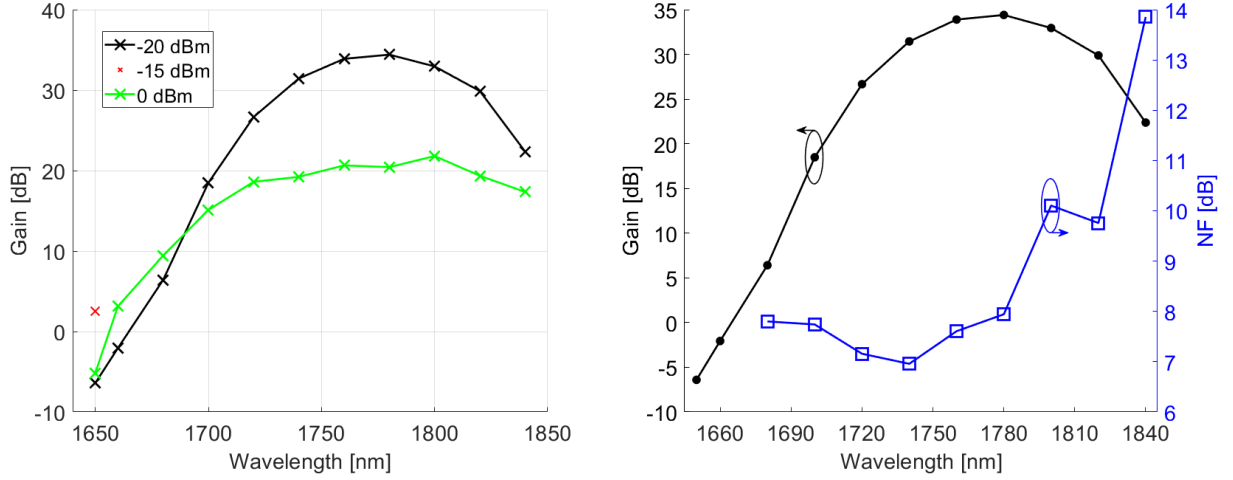


Figure 25: Left: TDFA-S-1565 gain with 1.9 W pump, lone point represents gain with -15 dBm input power and 3.2 W pump power; Right: TDFA-S-1565 gain and NF for -20 dBm input signal power and 1.9 W pump.

8.4 TDFA-S-1565 results

The TDFA-S setup represents a significant improvement in overall gain in the 1650-1800 nm range. The orders of magnitude more powerful pump, compared to the 790 nm LD, is able to successfully achieve high enough inversion to support gain of >15 dB at 1700 nm. The results of gain measurement with -20 dBm and 0 dBm input power are presented in Figure 25, left. The measurement window was extended to 1840 nm to provide overlap with TDFA-L. Signal gain of 2.53 dB at 1650 nm was achieved using a favorable combination of input and pump powers of -15 dBm and 3.23 W respectively. Gain and NF measurement results for -20 dBm input power are displayed in Figure 25, right. Various lengths of TDF and bend patterns were also tested. In this case, the bend radius and bend pattern significantly influence the gain at specific wavelengths, since the ASE now can become strong enough to deplete the inversion. The gain enhancement is highly variable and the exact way to bend the fiber to achieve the best performance requires further study, which is outside the scope of this work. An analysis of more sophisticated bending patterns can in principle be carried out using the same BPM toolkit which has been used to engineer

the depressed-cladding fiber in the first place. Calculating the wavelength dependent loss and using this information in a general TDFA model would be the ideal approach to optimizing this setup. Another avenue to explore relates to the recently studied thermal effects in TDFs. While these effects usually concern high power lasers, the dependence of Tm^{3+} absorption and emission cross-sections on temperature are more pronounced at shorter wavelengths [43]. Some sort of thermal management may be considered in future designs to, at least passively, enhance heat dissipation from the TDF. The insertion loss of optical components used in this setup increases rapidly towards 1840 nm, which is the primary cause for worsened noise performance towards the long wavelength edge of the gain spectrum.

8.5 TDFA-L results

The TDFA-L was found to have high gain covering the 1820-2020 nm range. Typical examples of spectral intensities obtained during gain and NF measurements are displayed in Figure 26, left. The maximum gain obtained for varying signal input power is displayed in Figure 26, right. Maximum small signal gain of 40.7 dB was measured at 1880 nm. A relatively flat gain spectrum of ~ 25 dB covering 140 nm in the 1840-1980 nm range was measured with 0 dBm input signal power. Those characteristics are a good compromise between short and long wavelength operation. Gain outside of the 1820-2020 nm window in this setup was considered too small to be useful and not studied further. The dependence of gain and NF on pump power for selected wavelengths is displayed in Figure 27, left. The NF stays relatively constant with increasing pump power. The gain, on the other hand, slowly saturates with increasing pump power. The NF tends to rise rapidly towards the edges of the gain spectrum, more pronouncedly on the short wavelength side, as is evident from Figure 27, right. The deterioration of gain and NF characteristics at both edges of the gain spectrum can be attributed to several factors. First and foremost, the length of the active fiber plays a crucial role in determining the gain spectrum. High inversion is necessary to achieve signal gain at shorter wavelengths, where the Tm^{3+} energy system

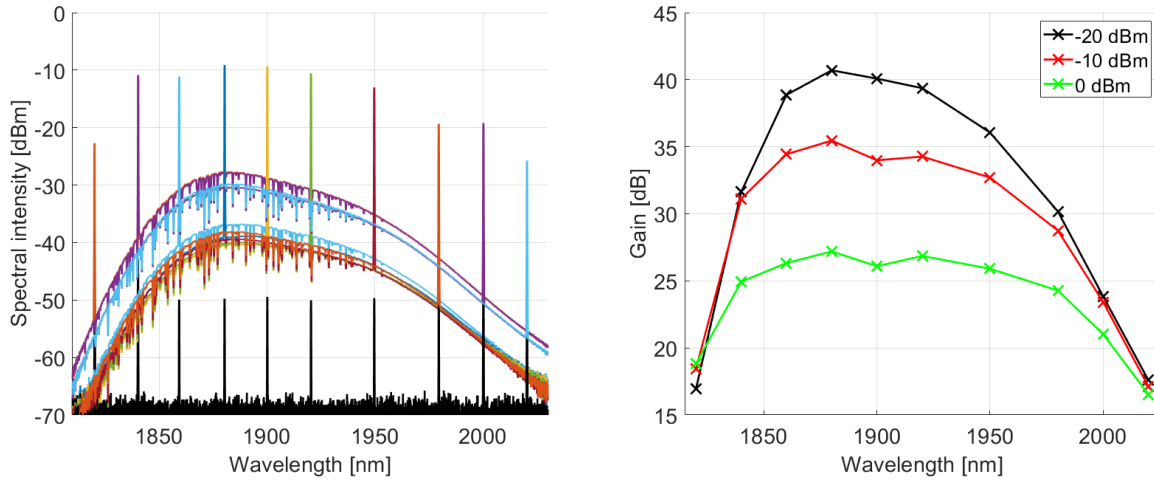


Figure 26: Left: Typical TDFA-L output spectra; Right: Amplifier gain characteristics versus wavelength.

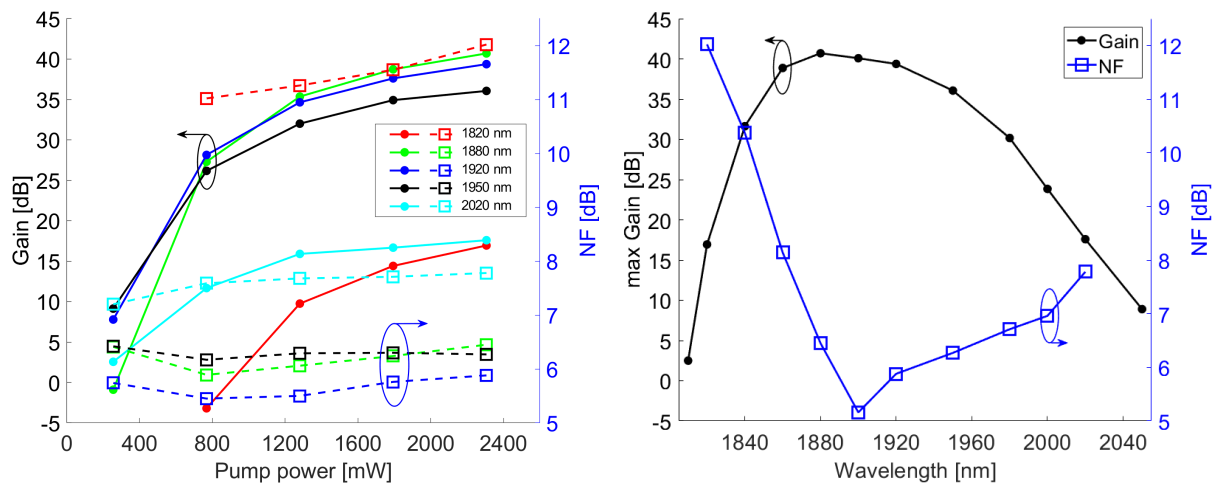


Figure 27: Gain and NF characteristics; Left: evolution of gain and NF with increasing pump power; Right: Maximum gain and corresponding NF at different wavelengths.

exhibits strong three-level behavior, leading to strong reabsorption at the unpumped end of the TDF. A shorter length of TDF must be used to ensure high enough inversion across the whole length of the fiber. Reabsorption is minimal at longer wavelengths; the Tm^{3+} emission cross section is, however, also small [43]. The amplifier thus achieves higher gain at longer wavelengths with a longer TDF. These two requirements are contradictory and, as mentioned previously, a compromise must be made in this case. The possibility of using counter-propagating amplified spontaneous emission to pump a short pre-amplifier section may be one way to improve performance as the relatively strong backwards ASE is currently wasted. Secondly, the useful operating window of optical components is limited, and insertion loss tends to increase exponentially at the edges of this window. With most of the components used having a design wavelength of either 1950 nm or 2000 nm (3.6 dB overall loss), the insertion loss especially towards 1800 nm (7.4 dB overall loss) increases rapidly hampering both gain and NF. This issue could be solved by developing custom optical components more suited for the gain window of the amplifier. Lastly, the attenuation and bend induced losses of the SMF28 fiber used increase rapidly at wavelengths >2000 nm. A complete redesign of all components and the TDF for the use with a more optimized single mode fiber would be the best solution to this issue. In the meantime, extra attention must be paid to the fiber bend radius to limit bend induced losses.

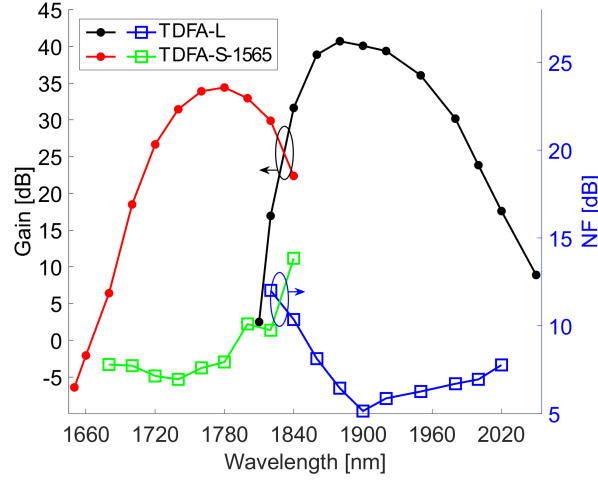


Figure 28: Combined gain and NF curves of TDFA-S-1565 and TDFA-L for -20 dBm input power.

8.6 Combining the setups

By combining the gain and NF curves obtained from TDFA-S-1565 and TDFA-L, displayed in Figure 28, it is possible to cover the 1740-1980 nm waveband with gain >30 dB at -20 dBm input power using just two amplifier setups. Further optimization could allow the use of both setups sharing a split pump source in a single system with bandwidth exceeding 20 THz, which is quite respectable by today's standards. This system could potentially support ~ 200 channels with 100 GHz spacing in a WDM system.

9 Conclusions

In conclusion, depressed-cladding TDF was designed and then manufactured using MCVD and nanoparticle doping methods. The bend-induced losses of the TDF were measured and discussed. The results of this measurement were used to help build a TTDFL covering wavelengths 1650-1800 nm. Another TTDFL, utilizing a standard step-index TDF, for the 1810-2050 nm range was built to provide overall coverage for the whole 1650-2050 nm range. The tunable sources provide signal of sufficient strength and quality for amplifier characterization purposes. Three TDFA setups were built, two of them covering the 1650-1800 nm range and one covering the 1800-2050 nm range. The viability of the depressed-cladding TDF was verified for use in TDFAs, successfully enhancing gain at wavelengths below 1800 nm. The TDFA for the 1650-1800 nm range has a high gain region between 1740 nm and 1840 nm providing relatively flat gain spectrum for input signals of ~ 0 dBm. Gain at 1650 nm is achievable with this setup, provided a favorable combination of input and pump power is selected. The TDFA for the 1800-2050 nm range has a high gain region between 1840 nm and 1980 nm providing relatively flat gain spectrum for input signals of ~ 0 dBm. Maximum small signal gain of 40.7 dB was measured at 1880 nm, in line with similar published research. Combining two TDFA setups may yield a device covering 1740-1980 nm corresponding to a ~ 20 THz bandwidth. The goals of this thesis have been met. Further improvements to the TDFA setups were discussed. Further research in this area might include a more detailed study of bend pattern enhancing ASE filtering in depressed-cladding TDFs, development of optical components more suited for the gain windows of the TDFAs, study of thermal effects on short wavelength gain performance in TDFs and development of more sophisticated modelling tools that consider the bend-induced losses in depressed cladding TDFs. Parts of this work were presented at the SPIE Photonics Europe 2022 conference in Strasbourg, France [Appendix A] and the SPIE Optics + Optoelectronics 2023 conference in Prague, Czechia [Appendix B]. Another part of this work was accepted for presentation at the CLEO/Europe-EQEC 2023 conference in Munich, Germany [Appendix C].

List of Figures

1	Simulation of depressed-cladding fiber; Left: 1D refractive index profile model; Right: calculated fiber losses for one loop with 3 cm radius at several wavelengths.	16
2	Measured refractive index profiles; Left: SG1797-43; Right: SG1797-443. .	17
3	Block diagram of amplifier gain measurement using an OSA; AMP: Amplifier.	19
4	Amplifier output optical power measured using an OSA.	20
5	Signal degradation due to amplifier produced noise; a) Transmitter output with SNR as limited by laser relative intensity noise (RIN); b) Received signal corrupted by beat, multipath interference and shot noise. Reproduced with permission from [36].	21
6	Optical spectra for source subtraction method of noise figure measurement; a) incident signal and SSE; b) output spectrum. Reproduced with permission from [36].	27
7	Input signal and laser spontaneous emission rejection using polarization extinction. Reproduced with permission from [36].	28
8	Attenuation measurements of SG1797 fiber; Left: measurement of ~ 11 cm of straight FUT to determine Tm^{3+} doping concentration; Right: Measurement of ~ 1 m long FUT to determine excess loss near the absorption band.	30
9	Detail of FUT bend loss near the Tm^{3+} absorption band; clover: the whole FUT is coiled with $R = 4.3$ cm and then deformed at four points distributed in a cross pattern with each attachment point being 3.25 cm from the center; fig8: one loop of fiber with $R = 8$ cm is made and then twisted into a symmetrical figure 8 shape.	31
10	FUT bend shapes.	31
11	TTDFL-S experimental setup; DG: diffraction grating; L: aspheric lens; OC: output coupler.	33

12	TTDFL-L experimental setup; DG: diffraction grating; L: aspheric lens; OC: output coupler.	33
13	TTDFL characterization scheme; OSC: oscilloscope.	34
14	TDFA-S-790 experimental setup; AMP: amplifier; ISO: optical isolator. . .	36
15	TDFA-S-1565 experimental setup, note the TDF bend shape used in this setup; AMP: amplifier; ISO: optical isolator.	37
16	TDFA-L experimental setup; AMP: amplifier; ISO: isolator.	38
17	TDFA gain and NF measurement; AMP: amplifier; PM: power meter. . . .	40
18	TTDFL-S output spectra at maximum pump power. Inset measured using ANDO AQ6317.	41
19	Left: TTDFL-S evolution of maximum output power over the covered range; Right: graphical description of TDF bend optimization.	42
20	Oscilloscope traces displaying the operating regimes of the TTDFL-S; Top: at maximum pump power; Bottom: at laser threshold.	43
21	TTDFL-L output spectra at maximum pump power.	45
22	TTDFL-L evolution of maximum output power over the covered range. . .	45
23	Oscilloscope traces displaying the operating regimes of the TTDFL-L; Top: at laser threshold; Bottom: at maximum pump power.	46
24	TDFA-S-790 gain.	47
25	Left: TDFA-S-1565 gain with 1.9 W pump, lone point represents gain with -15 dBm input power and 3.2 W pump power; Right: TDFA-S-1565 gain and NF for -20 dBm input signal power and 1.9 W pump.	48
26	Left: Typical TDFA-L output spectra; Right: Amplifier gain characteristics versus wavelength.	50
27	Gain and NF characteristics; Left: evolution of gain and NF with increasing pump power; Right: Maximum gain and corresponding NF at different wavelengths.	50
28	Combined gain and NF curves of TDFA-S-1565 and TDFA-L for -20 dBm input power.	52

References

- [1] WINZER, P. J., NEILSON, D. T., CHRAPLYVY, A. R.: Fiber-optic transmission and networking: the previous 20 and the next 20 years [Invited], *Optics Express*, 2018, **vol. 26(18)**, pp. 24190–24239, doi:10.1364/OE.26.024190.
- [2] VOJTECH, J., RADIL, J., HAVLIS, O., ALTMANN, M., SKODA, P., SMOTLACHA, V.: Resilience of semiconductor optical amplifier with holding beam injection to reflections in bidirectional reciprocal operation, in *2016 18th International Conference on Transparent Optical Networks (ICTON)*, IEEE, Trento, Italy, ISBN 978-1-5090-1467-5, ISSN 2161-2064, 2016 pp. 1–3, doi:10.1109/ICTON.2016.7550629.
- [3] FIRSTOV, S. V., KHEGAI, A. M., KHARAKHORDIN, A. V., ALYSHEV, S. V., FIRSTOVA, E. G., OSOSKOV, Y. J., MELKUMOV, M. A., ISKHAKOVA, L. D., EVLAMPIEVA, E. B., LOBANOV, A. S., YASHKOV, M. V., GURYANOV, A. N.: Compact and efficient O-band bismuth-doped phosphosilicate fiber amplifier for fiber-optic communications, *Scientific Reports*, 2020, **vol. 10(1)**, p. 11347, ISSN 2045-2322, doi:10.1038/s41598-020-68243-4.
- [4] BELARDI, W., KNIGHT, J. C.: Hollow antiresonant fibers with reduced attenuation, *Optics Letters*, 2014, **vol. 39(7)**, pp. 1853–1856, doi:10.1364/OL.39.001853.
- [5] BRADLEY, T. D., HAYES, J. R., CHEN, Y., JASION, G. T., SANDOGHCHI, S. R., SLAVIK, R., FOKOUA, E. N., BAWN, S., SAKR, H., DAVIDSON, I., TARANTA, A., THOMAS, J. P., PETROVICH, M. N., RICHARDSON, D., POLETTI, F.: Record low-loss 1.3dB/km data transmitting antiresonant hollow core fibre, in *2018 European Conference on Optical Communication (ECOC)*, IEEE, Rome, Italy, ISBN 978-1-5386-4862-9, ISSN 18265400, 2018 pp. 1–3, doi:10.1109/ECOC.2018.8535324.
- [6] WANG, J., LIANG, S., KANG, Q., JUNG, Y., UL ALAM, S., RICHARDSON, D. J.: Broadband silica-based thulium doped fiber amplifier employing multi-wavelength

- pumping, *Optics Express*, 2016, **vol. 24(20)**, pp. 23001–23008, doi:10.1364/OE.24.023001.
- [7] TENCH, R. E., ROMANO, C., DELAVALUX, J.-M.: Multistage single clad 2 μm TDFA with a shared L-band pump source, *Applied Optics*, 2018, **vol. 57(21)**, pp. 5948–5955, doi:10.1364/AO.57.005948.
- [8] AGGER, S. D., POVLSEN, J. H.: Emission and absorption cross section of thulium doped silica fibers, *Optics Express*, 2006, **vol. 14(1)**, pp. 50–57, ISSN 1094-4087, doi:10.1364/OPEX.14.000050.
- [9] TOWNSEND, J. E., BARNES, W. L., CRUBB, S. G.: Yb³⁺ sensitised Er³⁺ doped silica optical fibre with ultra high transfer efficiency and gain, *MRS Proceedings*, 1991, **vol. 1991(244)**, pp. 143–147, ISSN 0272-9172, doi:10.1557/PROC-244-143.
- [10] PODRAZKY, O., KASIK, I., POSPISILOVA, M., MATEJEC, V.: Use of alumina nanoparticles for preparation of erbium-doped fibers, in *LEOS 2007 - IEEE Lasers and Electro-Optics Society Annual Meeting Conference Proceedings*, IEEE, Lake Buena Vista, FL, USA, ISBN 978-1-4244-0924-2, ISSN 1092-8081, 2007 pp. 246–247, doi:10.1109/LEOS.2007.4382369.
- [11] CAJZL, J., PETERKA, P., KOWALCZYK, M., TARKA, J., SOBON, G., SOTOR, J., AUBRECHT, J., HONZÁTKO, P., KAŠÍK, I.: Thulium-doped silica fibers with enhanced fluorescence lifetime and their application in ultrafast fiber lasers, *Fibers*, 2018, **vol. 6(3)**, p. 66, ISSN 2079-6439, doi:10.3390/fib6030066.
- [12] KAMRADEK, M., HONZATKO, P., KASIK, I., AUBRECHT, J., MRAZEK, J., PODRAZKY, O., CAJZL, J., VARAK, P., KUBECEK, V., PETERKA, P.: Nanoparticle and solution doping for efficient holmium fiber lasers, *IEEE Photonics Journal*, 2019, **vol. 11(5)**, pp. 1–10, ISSN 1943-0655, doi:10.1109/JPHOT.2019.2940747.
- [13] MRÁZEK, J., SURÝNEK, M., BAKARDJIEVA, S., BURŠÍK, J., PROBOŠTOVÁ, J., KAŠÍK, I.: Luminescence properties of nanocrystalline europium titanate Eu₂Ti₂O₇,

- Journal of Alloys and Compounds*, 2015, **vol. 645**, pp. 57–63, ISSN 0925-8388, doi: 10.1016/j.jallcom.2015.05.019.
- [14] BAKER, C. C., FRIEBELE, E. J., BURDETT, A. A., RHONEHOUSE, D. L., FONTANA, J., KIM, W., BOWMAN, S. R., SHAW, L. B., SANGHERA, J., ZHANG, J., PATTNAIK, R., DUBINSKII, M., BALLATO, J., KUCERA, C., VARGAS, A., HEMMING, A., SIMAKOV, N., HAUB, J.: Nanoparticle doping for high power fiber lasers at eye-safer wavelengths, *Optics Express*, 2017, **vol. 25(12)**, ISSN 1094-4087, doi: 10.1364/OE.25.013903.
- [15] VAŘÁK, P., MRÁZEK, J., BLANC, W., AUBRECHT, J., KAMRÁDEK, M., PODRAZKÝ, O.: Preparation and properties of Tm-doped SiO₂-ZrO₂ phase separated optical fibers for use in fiber lasers, *Optical Materials Express*, 2020, **vol. 10(6)**, pp. 1383–1391, ISSN 2159-3930, doi:10.1364/OME.394068.
- [16] LI, Z., HEIDT, A. M., DANIEL, J. M. O., JUNG, Y., ALAM, S. U., RICHARDSON, D. J.: Thulium-doped fiber amplifier for optical communications at 2 μm, *Optics Express*, 2013, **vol. 21(8)**, pp. 9289–9297, doi:10.1364/OE.21.009289.
- [17] ISHII, S., MIZUTANI, K., FUKUOKA, H., ISHIKAWA, T., PHILIPPE, B., IWAI, H., AOKI, T., ITABE, T., SATO, A., ASAI, K.: Coherent 2 μm differential absorption and wind lidar with conductively cooled laser and two-axis scanning device, *Applied Optics*, 2010, **vol. 49(10)**, pp. 1809–1817, ISSN 0003-6935, doi:10.1364/AO.49.001809.
- [18] SINCORE, A., BRADFORD, J. D., COOK, J., SHAH, L., RICHARDSON, M. C.: High average power thulium-doped silica fiber lasers: Review of systems and concepts, *IEEE Journal of Selected Topics in Quantum Electronics*, 2018, **vol. 24(3)**, pp. 1–8, ISSN 1558-4542, doi:10.1109/JSTQE.2017.2775964.
- [19] MINGAREEV, I., WEIRAUCH, F., OLOWINSKY, A., SHAH, L., KADWANI, P., RICHARDSON, M.: Welding of polymers using a 2 μm thulium fiber laser, *Op-*

- tics & Laser Technology*, 2012, **vol. 44(7)**, pp. 2095–2099, ISSN 00303992, doi:10.1016/j.optlastec.2012.03.020.
- [20] SWIDERSKI, J., MICHALSKA, M., MAZE, G.: Mid-IR supercontinuum generation in a ZBLAN fiber pumped by a gain-switched mode-locked Tm-doped fiber laser and amplifier system, *Optics Express*, 2013, **vol. 21(7)**, pp. 7851–7857, doi:10.1364/OE.21.007851.
- [21] CHEUNG, C. S., DANIEL, J. M. O., TOKURAKAWA, M., CLARKSON, W. A., LIANG, H.: High resolution fourier domain optical coherence tomography in the 2 μ m wavelength range using a broadband supercontinuum source, *Optics Express*, 2015, **vol. 23(3)**, pp. 1992–2001, doi:10.1364/OE.23.001992.
- [22] JACKSON, S. D.: Towards high-power mid-infrared emission from a fibre laser, *Nature Photonics*, 2012, **vol. 6(7)**, pp. 423–431, ISSN 1749-4885, doi:10.1038/nphoton.2012.149.
- [23] MICHALSKA, M., BROJEK, W., RYBAK, Z., SZNELEWSKI, P., MAMAJEK, M., SWIDERSKI, J.: Highly stable, efficient Tm-doped fiber laser—a potential scalpel for low invasive surgery, *Laser Physics Letters*, 2016, **vol. 13(11)**, pp. 115101–115105, ISSN 1612-2011, doi:10.1088/1612-2011/13/11/115101.
- [24] KASAMATSU, T., YANO, Y., ONO, T.: Laser-diode-pumped highly efficient gain-shifted thulium-doped fiber amplifier operating in the 1480-1510-nm band, *IEEE Photonics Technology Letters*, 2001, **vol. 13(5)**, pp. 433–435, ISSN 1041-1135, doi:10.1109/68.920742.
- [25] LI, Z., HEIDT, A. M., SIMAKOV, N., JUNG, Y., DANIEL, J. M. O., ALAM, S. U., RICHARDSON, D. J.: Diode-pumped wideband thulium-doped fiber amplifiers for optical communications in the 1800 - 2050 nm window, *Optics Express*, 2013, **vol. 21(22)**, pp. 26450–26455, doi:10.1364/OE.21.026450.

- [26] LI, Z., JUNG, Y., DANIEL, J. M. O., SIMAKOV, N., SHARDLOW, P. C., HEIDT, A. M., CLARKSON, W. A., ALAM, S. U., RICHARDSON, D. J.: Extreme short wavelength operation (1.65 - 1.7 μm) of silica-based thulium-doped fiber amplifier, in *Optical Fiber Communication Conference*, OSA, Washington, D.C, ISBN 978-1-55752-937-4, 2015 p. Tu2C.1, doi:10.1364/OFC.2015.Tu2C.1.
- [27] JUNG, Y., LI, Z., SIMAKOV, N., DANIEL, J. M. O., JAIN, D., SHARDLOW, P. C., HEIDT, A. M., SAHU, J. K., HEMMING, A., CLARKSON, W. A., ALAM, S. U., RICHARDSON, D. J.: Silica-based thulium doped fiber amplifiers for wavelengths beyond the L-band, in *2016 Optical Fiber Communications Conference and Exhibition (OFC)*, 2016 pp. 1–3.
- [28] CHEN, S., JUNG, Y., UL ALAM, S., RICHARDSON, D. J., SIDHARTHAN, R., HO, D., YOO, S., DANIEL, J. M. O.: Ultra-short wavelength operation of thulium-doped fiber amplifiers and lasers, *Optics Express*, 2019, **vol. 27(25)**, pp. 36699–36707, ISSN 1094-4087, doi:10.1364/OE.27.036699.
- [29] PETERKA, P., KAŠÍK, I., MATĚJEC, V., BLANC, W., FAURE, B., DUSSARDIER, B., MONNOM, G., KUBEČEK, V.: Thulium-doped silica-based optical fibers for cladding-pumped fiber amplifiers, *Optical Materials*, 2007, **vol. 30(1)**, pp. 174–176, ISSN 09253467, doi:10.1016/j.optmat.2006.11.039.
- [30] LANCASTER, D. G., SABELLA, A., HEMMING, A., BENNETTS, S., JACKSON, S. D.: Power-scalable thulium and holmium fibre lasers pumped by 793 nm diode lasers, in *Advanced Solid-State Photonics*, OSA, Washington, D.C, ISBN 1-55752-829-2, 2007 pp. WE5–, doi:10.1364/ASSP.2007.WE5.
- [31] YEH, C.-H., LEE, C.-C., CHI, S.: A tunable S-band erbium-doped fiber ring laser, *IEEE Photonics Technology Letters*, 2003, **vol. 15(8)**, pp. 1053–1054, ISSN 1041-1135, doi:10.1109/LPT.2003.815314.

- [32] VINCETTI, L., FORONI, M., POLI, F., MAINI, M., CUCINOTTA, A., SELLERI, S., ZOBOLI, M.: Numerical modeling of S-band EDFA based on distributed fiber loss, *Journal of Lightwave Technology*, 2008, **vol. 26(14)**, pp. 2168–2174, ISSN 0733-8724, doi:10.1109/JLT.2008.923221.
- [33] PETERKA, P.: *Dvoujádrová optická vlákna pro vláknové lasery*, Disertační práce, České vysoké učení technické v Praze, Praha, 1999.
- [34] VEETIKAZHY, M., HANSEN, A. K., MARTI, D., JENSEN, S. M., BORRE, A. L., ANDRESEN, E. R., DHOLAKIA, K., ANDERSEN, P. E.: BPM-Matlab, *Optics Express*, 2021, **vol. 29(8)**, pp. 11819–11832, ISSN 1094-4087, doi:10.1364/OE.420493.
- [35] HUI, R., O’SULLIVAN, M.: *Fiber optic measurement techniques*, Academic Press, San Diego, CA, 1st ed., 2008, ISBN 9780123738653, doi:10.1016/b978-0-12-373865-3.x0001-8.
- [36] BANEY, D. M., GALLION, P., TUCKER, R. S.: Theory and measurement techniques for the noise figure of optical amplifiers, *Optical Fiber Technology*, 2000, **vol. 6(2)**, pp. 122–154, ISSN 10685200, doi:10.1006/ofte.2000.0327.
- [37] Yokogawa Test & Measurement Corporation: *OSA: Optical Amplifier (EDFA) Measurement Guide*, 2022, URL https://cdn.tmi.yokogawa.com/1/9425/files/AF106_OSA_Optical_Amplifier_EDFA_measurement_guide_EN_R0_r1.pdf.
- [38] POKORNÝ, J., MORAVEC, O., AUBRECHT, J.: Broadband fiber-optic thulium-doped source of amplified spontaneous emission, in *Proc.SPIE*, vol. 11773, 2021 p. 117731D, doi:10.1117/12.2592931.
- [39] PÍSAŘÍK, M., PETERKA, P., ZVÁNOVEC, S., BARAVETS, Y., TODOROV, F., KAŠÍK, I., HONZÁTKO, P.: Fused fiber components for “eye-safe” spectral region around 2 μm , *Optical and Quantum Electronics*, 2014, **vol. 46(4)**, pp. 603–611, ISSN 1572-817X, doi:10.1007/s11082-013-9801-2.

- [40] AUBRECHT, J., PETERKA, P., HONZÁTKO, P., MORAVEC, O., KAMRÁDEK, M., KAŠÍK, I.: Broadband thulium-doped fiber ASE source, *Optics Letters*, 2020, vol. **45(8)**, pp. 2164–2167, ISSN 0146-9592, doi:10.1364/OL.389397.
- [41] POKORNÝ, J.: *Širokopásmový opticko-vláknový thuliem dopovaný zdroj zesílené spontánní emise*, Bakalářská práce, České vysoké učení technické v Praze, Praha, 2021.
- [42] POKORNÝ, J., AUBRECHT, J., PETERKA, P., BUNGE, C.-A., KALLI, K., PETERKA, P.: Broadband fiber-optic thulium-doped amplifier for wavelengths beyond the L-band, in *Micro-Structured and Specialty Optical Fibres VII*, SPIE, Strassburg, ISBN 9781510651562, 2022 p. 1214009, doi:10.1117/12.2622428.
- [43] JIŘÍČKOVÁ, B., GRÁBNER, M., JAUREGUI, C., AUBRECHT, J., SCHREIBER, O., PETERKA, P.: Temperature-dependent cross section spectra for thulium-doped fiber lasers, *Optics Letters*, 2023, vol. **48(3)**, pp. 811–814, ISSN 0146-9592, doi:10.1364/OL.479313.

Abstract

The subject of this thesis is the development and characterization of thulium-doped fiber optic amplifiers (TDFA) for wavelengths beyond the L-band (1565-1625 nm) which includes tunable thulium-doped fiber lasers (TTDFL) needed to characterize the TDFAs. Also included is the development on novel geometry thulium doped fiber featuring a depressed cladding around the core of the fiber. This geometry introduces a fundamental mode cutoff to the fiber, which can be adjusted by bending the fiber. The dependence of fundamental mode cutoff wavelength is investigated and the results used to setup a TTDFL and two TDFAs for wavelengths covering 1650-1800 nm. Together with a TTDFL and a TDFA for wavelengths spanning 1800-2050 nm these devices form the focus and final product of this thesis. The TTDFLs must meet certain requirements to be used for amplifier characterization such as sufficient output power, output power stability, signal to noise ratio and tuning range. Measurements confirming the compliance with these requirements are described and their results presented. The TDFAs are characterized over a number of wavelengths in their intended coverage range with measurements determining gain and, in case the setup is deemed viable for use in real world applications, also the noise figure. A discussion pertaining possible causes for issues and further improvements is contained at the end of each result section. Of significant note are the results of the TDFA covering 1800-2050 nm, where good amplifier performance spanning 1840-1980 nm is observed with a relatively flat gain spectrum of ~ 25 dB with input signal power of 0 dBm. Maximum small signal gain reached with this setup was 40.7 dB with corresponding noise figure of 6.45 dB at 1880 nm. Relatively good results were also achieved with the TDFA setup covering 1650-1800 nm, where high gain covering 1740-1840 nm was observed. This allows for a two-device system covering 1740-1980 nm corresponding to a ~ 20 THz bandwidth.

Abstrakt

Předmětem této práce je vývoj a charakterizace thuliem dopovaných opticky vláknových zesilovačů (TDFA) pro vlnové délky za pásmem L (1565-1625 nm) k čemuž také přísluší laditelné thuliem dopované vláknové lasery (TTDFL) potřebné pro charakterizaci TDFA. K práci dále náleží vývoj thuliem dopovaného vlákna s novou geometrií, která zahrnuje vnitřní plášť s poklesem indexu lomu okolo jádra. Tato geometrie umožňuje vyvázat základní mód vlákna o vlnové délce delší než té, která je nastavena ohybem vlákna. Závislost tohoto jevu na ohybu vlákna je nejdříve prostudována a tyto poznatky jsou následně využity při sestavení TTDFL a dvou TDFA pro vlnové délky 1650-1800 nm. Spolu s TTDFL a TDFA pro vlnové délky 1800-2050 nm tvoří tyto zařízení hlavní náplň a zároveň výsledný produkt této práce. TTDFL zdroje musí splňovat určité požadavky, aby bylo možné je použít pro charakterizaci TDFA. Mezi tyto požadavky patří dostatečný výstupní výkon, stabilita výstupního výkonu, poměr signálu k šumu a rozsah laditelnosti. Splnění těchto požadavků je ověřeno experimenty, které jsou popsány a vyhodnoceny. TDFA jsou charakterizovány na několika vlnových délkách pokrývajících jejich zamýšlené pásmo vlnových délek. Charakterizace zahrnuje měření zesílení a v případě, kdy je zařízení případně možné nasadit do reálné aplikace, je provedeno měření šumového čísla. Na konci každé sekce s výsledky jsou diskutovány příčiny některých komplikací a také jsou navržena možná vylepšení. Lze zmínit výsledky měření TDFA pro vlnové délky 1800-2050 nm, kdy naměřené zesílení v pásmu 1840-1980 nm vykazovalo plochou charakteristiku s hodnotou okolo 25 dB pro vstupní signál o výkonu 0 dBm. Maximálního malosignálového zesílení bylo dosaženo na vlnové délce 1880 nm, kde byla naměřena hodnota zesílení 40,7 dB a k tomu příslušné šumové číslo 6,45 dB. Relativně dobrých výsledků bylo dosaženo s TDFA pro vlnové délky 1650-1800 nm, který vykazuje vysoké zesílení ve spektrální oblasti 1740-1840 nm. Kombinací dvou TDFA je tedy možné pokrýt oblast 1740-1980 nm, což odpovídá šířce pásma okolo 20 THz.

Appendices

A SPIE Photonics Europe 2022 Proceedings Article i

B SPIE Optics + Optoelectronics 2023 Proceedings Article ix

C CLEO/Europe-EQEC 2023 Contribution xvi

Appendix

A SPIE Photonics Europe 2022 Proceedings Article

PROCEEDINGS OF SPIE

[SPIDigitalLibrary.org/conference-proceedings-of-spie](https://spiedigitallibrary.org/conference-proceedings-of-spie)

Broadband fiber-optic thulium-doped amplifier for wavelengths beyond the L-band

Jan Pokorný, Jan Aubrecht, Pavel Peterka

Jan Pokorný, Jan Aubrecht, Pavel Peterka, "Broadband fiber-optic thulium-doped amplifier for wavelengths beyond the L-band," Proc. SPIE 12140, Micro-Structured and Specialty Optical Fibres VII, 1214009 (19 May 2022); doi: 10.1117/12.2622428

SPIE.

Event: SPIE Photonics Europe, 2022, Strasbourg, France

Broadband fiber-optic thulium-doped amplifier for wavelengths beyond the L-band

Jan Pokorný^{a,b}, Jan Aubrecht^a and Pavel Peterka^a

^aInstitute of Photonics and Electronics of the Czech Academy of Sciences, Chaberská 57, 182 51 Prague, Czech Republic

^bFaculty of Nuclear Sciences and Physical Engineering, Czech Technical University in Prague, Břehová 7, 115 19 Prague, Czech Republic

ABSTRACT

We present preliminary characterization of an optical fiber amplifier for wavelengths beyond the L-band based on a core-pumped thulium-doped fiber developed and fabricated in-house. We explore adaptation of an existing broadband fiber-optic thulium-doped source of amplified spontaneous emission, which generates radiation in a spectral region around 2 micrometer wavelengths, for the purpose of signal amplification. The amplifier is pumped by an erbium-doped fiber laser at 1566 nm in a backward configuration with respect to the pump power. We characterize the amplifier using a narrowband input signal at 1950 nm and 1996 nm. We optimize the amplifier setup by varying the length of the active fiber and pump power. Results show that amplification of >30 dB at 1950 nm with maximum output power ~ 300 mW is achievable with existing setups.

Keywords: Thulium, Fiber, Telecom, L-band, Silica, Fiber laser, Fiber-optic amplifier, Thulium-doped fiber

1. INTRODUCTION

Existing optical communication infrastructure is approaching its physical limits due to an exponential rise of data traffic over the years¹. The focus has so far been on improving upon existing technology and utilizing the available bandwidth in the most efficient way. Recent technological advances provide another avenue of data transmission rate growth by expanding the available bandwidth. The E-band (1360-1460 nm) and S-band (1460-1530 nm) are being examined for use with existing fiber optic networks utilizing semiconductor optical amplifiers². The spectral region beyond the L-band (1565-1610 nm), which may soon become viable for data transmission due to the development of low-loss anti resonant hollow-core optical fibers (AR-HCF)³, also shows a lot of potential in this area. AR-HCFs offer low transmission losses across a wide spectral range⁴ including the L-band and beyond as well as reduced latency and a host of other benefits associated with utilizing a hollow core compared to existing systems. The next logical step is to develop optical fiber amplifiers, covering the newly viable spectral regions, which mirror the success of existing amplifiers, such as erbium-doped fiber amplifiers (EDFA). Thulium-doped fiber amplifiers (TDFA) are of particular interest for application in the spectral region beyond the L-band showing promising results^{5,6}. TDFAs offer the widest gain band (window from ~ 1750 to ~ 2050 nm) amongst all rare earth doped fiber amplifiers providing further potential means to expand the overall fiber capacity. Thulium-doped fibers (TDF) yield fluorescence spanning the band from 1600 to 2200 nm and hence are an attractive gain medium for power scalable laser sources operating in this eye-safe wavelength range. The current shortcomings of silica TDFs, mainly the orders of magnitude shorter lifetime compared to erbium-doped silica fibers, are being addressed by the introduction of advanced manufacturing methods, such as nanoparticle doping^{7,8,9,10,11} that may further improve their performance. Further applications of TDFAs may include free-space optical communication¹² and gas sensing applications¹³, material processing applications¹⁴, pumping of solid state lasers and generation of supercontinuum¹⁵, optical coherence tomography¹⁶, or defense applications¹⁷. In this article, we investigate a TDFA for optical signal amplification in the spectral region beyond the L-band for telecom use. We present gain and output power characteristics at two selected wavelengths of 1950 nm and 1996 nm. The characteristics were measured in a setup with two lengths of the TDF gain medium of 2 m and 4 m. We optimize the length of the TDF for the selected pumping scheme.

Micro-Structured and Specialty Optical Fibres VII, edited by Kyriacos Kalli,
Pavel Peterka, Christian-Alexander Bunge, Proc. of SPIE Vol. 12140,
1214009 · © 2022 SPIE · 0277-786X · doi: 10.1117/12.2622428

Proc. of SPIE Vol. 12140 1214009-1

2. MATERIALS AND METHODS

We have previously demonstrated a thulium-doped fiber optic amplified spontaneous emission (Tm:ASE) source for the spectral region 1800-2000 nm with an output power of >130 mW. The Tm:ASE source has a broad emission spectrum of more than 140 nm at the -3 dB level with two local peaks at around 1850 nm and 1950 nm. The width and center of the emission spectrum can be optimized by varying the length of the active fiber or by varying the pump power, thus allowing for amplifier fine tuning^{18, 19}. This device serves as the basis for the development of a TDFA operating in this spectral region and was used to estimate the length of the TDF. The difference between the published Tm:ASE source and the TDFA is in removing of a metallic mirror, which served to reflect forward ASE for further amplification, and an addition of an optical isolator for the input signal. Both devices employ a simple all-fiber geometry utilizing commercially available optical components except for the active fiber. The experimental setup used for our TDFA is illustrated schematically in Figure 1a. An in-house-built erbium-doped fiber laser (EDFL) in a ring arrangement emitting at 1566 nm was applied as an in-band pumping source with a maximum output power around 2.3 W. This EDFL can be easily modified to an EDFA and utilized as an amplification module elsewhere. The pump power is coupled into the active fiber by a 1560/1950 nm wavelength division multiplexor (WDM). Backwards pumping with respect to the pump power was selected also due to the experience with the Tm:ASE source, which showed strong signal amplification in the backwards direction. As a gain medium we used a core-pumped highly doped TDF which was prepared in-house using the modified chemical vapor deposition method and solution doping method. Numerical modelling and experience with the Tm:ASE source were used to select the ~2 m and ~4 m lengths of the TDF for signal amplification. Optical isolators on both sides of the amplifier help suppress parasitic lasing and ensure the correct direction of power flow through the amplifier. A 95/5 coupler splits away a small part of the output signal for monitoring purposes. Some of the optical components were previously developed in collaboration with SQS Vláknová optika company²⁰.

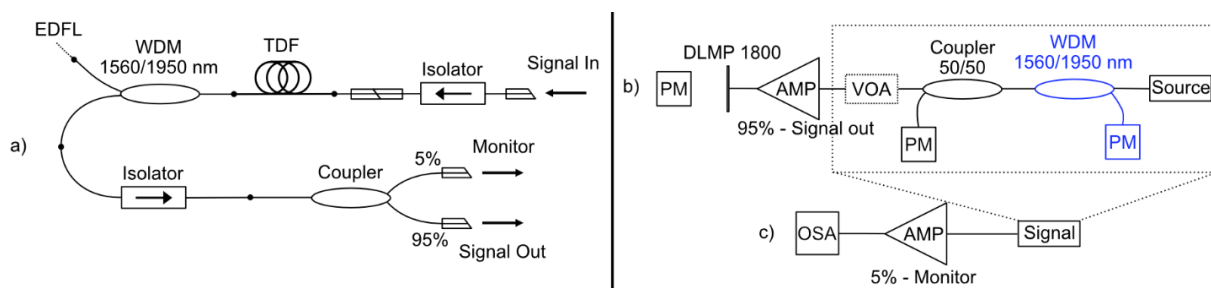


Figure 1: a) Experimental arrangement of the TDFA. b) Power measurement setup, optional unabsorbed pump power measurement components in blue, VOA used optionally to achieve microwatt levels of signal input power. PM: power meter, AMP: TDFA. c) Gain measurement using the OSA. The reference signal is measured after splitting and attenuation, accurately representing the signal at the input port of the amplifier.

First, the characteristics of the amplifier were measured using a simple output power measurement method. Two different devices were used to provide the input signal: an in-house built fiber laser at 1950 nm and a commercial discrete mode laser diode from Eblana Photonics emitting at 1996 nm. First the signal power at the input of the amplifier was measured using a power meter and then calibrated to another power measurement taken at one of the outputs of a 50/50 coupler. A variable optical attenuator (VOA) was used to attenuate the signal. A 1550/1950 WDM was inserted between the 50/50 coupler and the signal source to determine unabsorbed pump power emitted from the input port of the TDFA and prevent damage to the signal sources. The setup for power measurement is shown in Figure 1b. The output power was measured by a S405C Thorlabs thermopile detector or Thorlabs S148C integrating sphere photodiode power sensor and PM100D Thorlabs power meter. A Thorlabs DMLP 1800 longpass dichroic mirror located in front of the power detector was used to filter out shorter wavelengths of ASE. These measurements were used to select three general signal input power levels to characterize the TDFA. Signal power was chosen in the range from ~3 μ W to ~4 mW to evaluate amplification of both small and higher signals. Then a more accurate method of measuring the amplifier characteristics was employed and again, two different devices were used as input signal sources: an in-house built fiber laser at 1950 nm and a commercial discrete mode laser diode from Eblana Photonics emitting at 1996 nm. The input signal was attenuated using a VOA and a 50/50 coupler, the second port of which was used to monitor the signal power. The spectral and amplification characterization was performed using the Thermo Nicolet 8700 FTIR optical spectrum analyzer (OSA) with resolution of 1 cm^{-1} , i.e. 0.4 nm at 2000 nm. The block diagram of the measurement setup is shown in Figure 1c.

The gain was determined using a method, where the input and output spectral intensities are measured and then compared ²¹. This method allows gain measurement utilizing the higher dynamic range of an OSA than that of a power meter and doesn't require narrowband optical filters to accurately filter out ASE noise. The calculations were performed using software processing. A MATLAB script has been developed especially for this purpose which automatically detects narrowband peaks and calculates noise levels and gain based on user defined parameters. It should be mentioned that spectral intensity measurements were taken from the monitor port of the TDFA and subsequently adjusted using the known coupling ratio of the output coupler to match output signal power and spectral intensity present at the signal out port. This was done to obtain both the input and the output signal spectral intensities of similar magnitude and to eliminate potential inaccuracies in attenuation of the output signal, since the 95/5 output coupler of the TDFA has a known characteristic. Where possible, the interpolation method was used to determine the ASE noise level and the extrapolation method was used in cases where the dynamic range of the OSA was insufficient.

3. RESULTS AND DISCUSSION

Examples of spectral intensities obtained from the OSA measurements are displayed in Figure 2. High levels of ASE were observed when input signal power was of the order of microwatts. For higher signal input powers (hundreds of microwatts and higher) the ratio of the output signal intensity to ASE noise reached expected levels that, however, exceeded the dynamic range of the used OSA (only about 30 dB), which in turn made it impossible to accurately determine the ASE noise level. Therefore, for the preliminary TDFA tests presented here, the noise figure is not evaluated. The inaccuracy to gain measurement introduced due to this phenomenon is relatively small and can be neglected, since the noise level is several orders of magnitude lower than the output signal power.

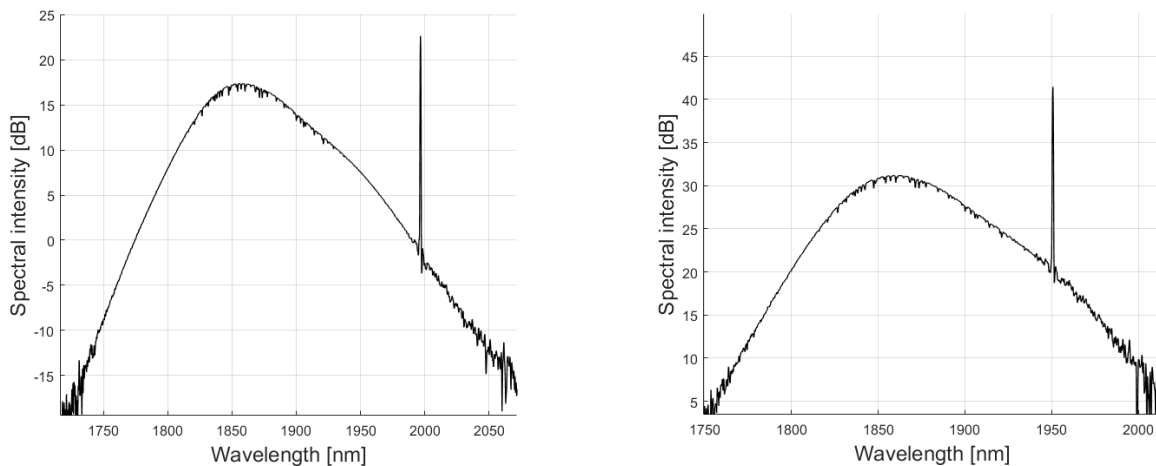


Figure 2 Typical TDFA output spectra for 2 m long TDF and 5 μ W signal power. Left: 1996 nm input signal, right: 1950 nm input signal.

The gain obtained for varying signal input power, pump power and length of the TDF is displayed in Figure 3. For the used pumping scheme, it is apparent that the chosen length of 2 m of the TDF can be considered optimal, showing overall higher gain than the 4 m long TDF, while at the same time low levels of unabsorbed pump power. Pump power absorption saturation can be observed for the 2 m long TDF and was registered in an increase of unabsorbed pump power present at the 1560 nm port of the 1560/1950 nm WDM. Gain saturation due to increasing pump power can also be observed for the 2 m long TDF. The maximum small signal gain obtained for the 2 m long TDF were 33.1 dB and 21.7 dB at 1950 nm and 1996 nm respectively.

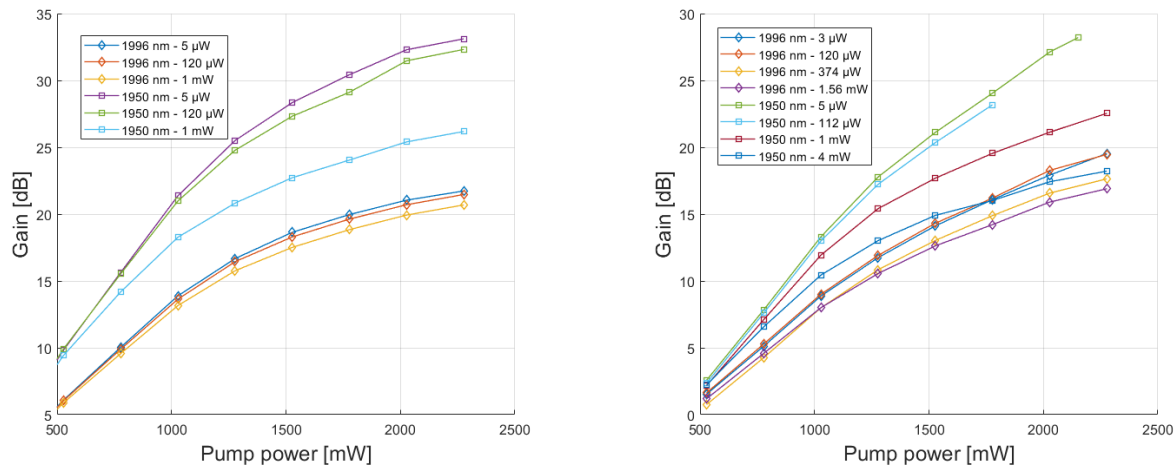


Figure 3 Amplifier gain characteristics versus pump power. Left: 2 m long TDF, right: 4 m long TDF.

When using the amplifier for higher power amplification the ASE noise power is negligible in comparison to the signal output power. Slope efficiency of the amplifier can therefore be easily obtained from the power measurements. For the 2 m long TDF the slope efficiency at 1950 nm was determined as 23 % and at 1996 nm at 5.6 %. For the 4 m long TDF the slope efficiency at 1950 nm was 19.1% and at 1996 nm 6.4 %. The slope was obtained by linear fitting in the linear region of the curves displayed in Figure 4. The increased slope efficiency at 1996 nm for the 4 m long TDF confirms our initial assumptions about the fiber length suitable for long wavelength amplification. It can be assumed that better results for 1996 nm amplification could be achieved by using the longer TDF and a more powerful pump laser.

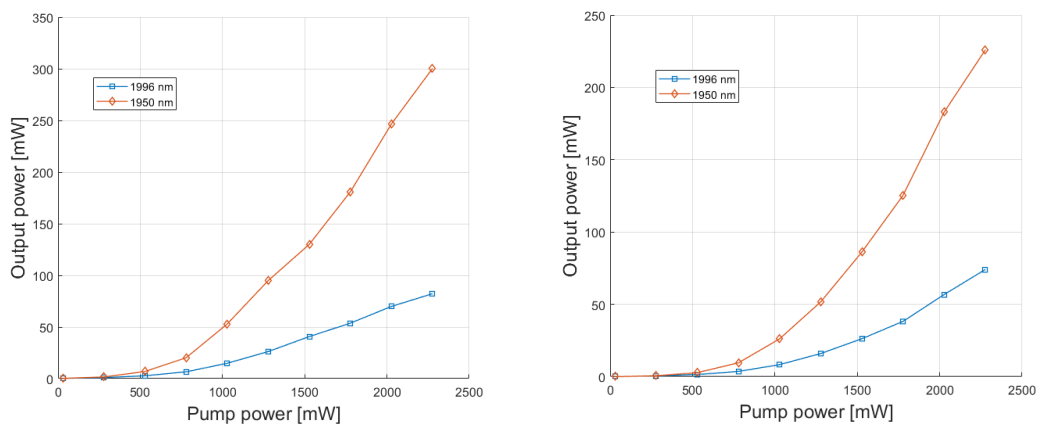


Figure 4 Output power for select signal input powers. Left: signal input power 868 μW at 1950 nm and 828 μW at 1996 nm for a 2 m long TDF. Right: signal input power 884 μW at 1950 nm and 840 μW at 1996 nm for a 4 m long TDF.

A brief summary of results regarding the gain characteristics of the TDFA is prepared in Table 1. The summary displays signal power levels in dBm grouping comparable signal power levels together to show expected performance of the amplifier over a range of signal input power that could be encountered in real applications. Due to the nature of the comparison, only values obtained at the same pump power level are included.

Table 1 General gain characteristics at 1.77 W pump power. Signal power is shown in dBm to give general idea of TDFA performance for signal input power of same magnitude.

TDF length [m]	Signal power [dBm]	Gain@1950 nm [dB]	Gain@1996 nm [dB]
2	-30	30.4	20.0
	-10	29.1	19.6
	0	24.0	18.8
4	-30	24.0	16.1
	-10	23.2	16.2
	0	19.5	14.2

To summarize the results, gain and power characterization of the TDFA for varying pump and signal power levels for a setup using a 2 and 4 m long TDF the optimal length for use with the EDFL pump was determined to be 2 m. The maximum gain achieved with this TDF was 33.1 dB and 21.7 dB at 1950 nm and 1996 nm respectively, the maximum power measured was ~300 mW at 1950 nm and ~80 mW at 1996 nm. The slope efficiency at 1996 nm was slightly better for the 4 m long TDF at 6.4 %, indicating possibly better gain characteristics at longer wavelengths if a more powerful pump is used. Some of the connections between the optical components have been facilitated by optical connectors which were usually accompanied by extra losses. The additional signal losses produced by these connectors and extra splices lead to lowered performance of the TDFA. Improving the EDFL pump is one of the possible performance enhancements to be investigated. The next planned step is the development of a thulium amplifier for the spectral region just beyond the L-band, which will be based on a modified optical fiber as well as on a modified pump source. The pumping source will be realized by a laser diode (LD) emitting around 790 nm. The advantage of direct LD pumping is simplicity of the amplifier; however, some tradeoffs are to be expected especially where LD cost and performance are considered.

4. CONCLUSIONS

In conclusion, we have reported preliminary results of a laboratory setup of a TDFA assembled from commercially available optical components and an in-house fabricated thulium-doped fiber. The TDFA setup was characterized for a range of signal and pump powers as well as for two lengths of the TDF. An optimal length of 2 m of the TDF was found for this setup and fiber. A maximum small signal gain of 33.1 dB at 1950 nm and 21.7 dB at 1996 nm was achieved. The performance of the amplifier can be further improved for example by optimizing the connections between the components or by improving the pump power and further fiber length optimization. The characterization shall be improved by using an OSA with higher dynamic range to also characterize the noise figure for all tested power and wavelength ranges. The gained results will aid in the field of TDFA development and possibly in the task of expanding available telecom bandwidth. Our future work will focus on TDFAs operating at shorter wavelengths by means of a modified pumping scheme and optimized fiber structure. This work was financially supported by the Development Fund of CESNET under project number 672/2021.

REFERENCES

- [1] Winzer, P., Neilson, D. and Chraplyvy, A., "Fiber-optic transmission and networking: the previous 20 and the next 20 years [Invited]," *Optics Express* **26**(18), 24190-24239 (2018).
- [2] Vojtech, J., Radil, J., Havlis, O., Altmann, M., Skoda, P. and Smotlacha, V., "Resilience of semiconductor optical amplifier with holding beam injection to reflections in bidirectional reciprocal operation" 2016 18th International Conference on Transparent Optical Networks (ICTON), 1-3, IEEE, Trento, Italy (2016).

- [3] Belardi, W. and Knight, J., "Hollow antiresonant fibers with reduced attenuation," *Optics Letters* **39**(7), 1853-1856 (2014).
- [4] Bradley, T., Hayes, J., Chen, Y., Jasion, G., Sandoghchi, S., Slavik, R., Fokoua, E., Bawn, S., Sakr, H., Davidson, I., Taranta, A., Thomas, J., Petrovich, M., Richardson, D. and Poletti, F., "Record Low-Loss 1.3dB/km Data Transmitting Antiresonant Hollow Core Fibre," 2018 European Conference on Optical Communication (ECOC), 1-3, IEEE, Rome, Italy (2018).
- [5] Wang, J., Liang, S., Kang, Q., Jung, Y., Alam, S. and Richardson, D., "Broadband silica-based thulium doped fiber amplifier employing multi-wavelength pumping," *Optics Express* **24**(20), 23001-23008 (2016).
- [6] Tench, R., Romano, C. and Delavaux, J., "Multistage single clad 2 μm TDFA with a shared L-band pump source," *Applied Optics* **57**(21), 5948-5955 (2018).
- [7] Podrazky, O., Kasik, I., Pospisilova, M. and Matejec, V., "Use of alumina nanoparticles for preparation of erbium-doped fibers," LEOS 2007 - IEEE Lasers and Electro-Optics Society Annual Meeting Conference Proceedings, 246-247, IEEE, Lake Buena Vista, FL, USA (2007).
- [8] Cajzl, J., Peterka, P., Kowalczyk, M., Tarka, J., Sobon, G., Sotor, J., Aubrecht, J., Honzátko, P. and Kašík, I., "Thulium-Doped Silica Fibers with Enhanced Fluorescence Lifetime and Their Application in Ultrafast Fiber Lasers," *Fibers* **6**(3), 66 (2018).
- [9] Kamradek, M., Honzátko, P., Kasik, I., Aubrecht, J., Mrazek, J., Podrazky, O., Cajzl, J., Varak, P., Kubecek, V. and Peterka, P., "Nanoparticle and Solution Doping for Efficient Holmium Fiber Lasers," *IEEE Photonics Journal* **11**(5), 1-10 (2019).
- [10] Mrázek, J., Surýnek, M., Bakardjieva, S., Buršík, J., Proboštová, J. and Kašík, I., "Luminescence properties of nanocrystalline europium titanate $\text{Eu}_2\text{Ti}_2\text{O}_7$," *Journal of Alloys and Compounds* **645**, 57-63 (2015).
- [11] Baker, C., Friebele, E., Burdett, A., Rhonehouse, D., Fontana, J., Kim, W., Bowman, S., Shaw, L., Sanghera, J., Zhang, J., Pattnaik, R., Dubinskii, M., Ballato, J., Kucera, C., Vargas, A., Hemming, A., Simakov, N. and Haub, J., "Nanoparticle doping for high power fiber lasers at eye-safer wavelengths," *Optics Express* **25**(12) (2017).
- [12] Li, Z., Heidt, A., Simakov, N., Jung, Y., Daniel, J., Alam, S. and Richardson, D., "Diode-pumped wideband thulium-doped fiber amplifiers for optical communications in the 1800 – 2050 nm window," *Optics Express* **21**(22), 26450-26455 (2013).
- [13] McComb, T., Sims, R., Willis, C., Kadwani, P., Sudesh, V., Shah, L. and Richardson, M., "High-power widely tunable thulium fiber lasers," *Applied Optics* **49**(32), 6236-6242 (2010).
- [14] Sincore, A., Bradford, J., Cook, J., Shah, L. and Richardson, M., "High Average Power Thulium-Doped Silica Fiber Lasers: Review of Systems and Concepts," *IEEE Journal of Selected Topics in Quantum Electronics* **24**(3), 1-8 (2018).
- [15] Swiderski, J., Michalska, M. and Maze, G., "Mid-IR supercontinuum generation in a ZBLAN fiber pumped by a gain-switched mode-locked Tm-doped fiber laser and amplifier system," *Optics Express* **21**(7), 7851-7857 (2013).
- [16] Cheung, C., Daniel, J., Tokurakawa, M., Clarkson, W. and Liang, H., "High resolution Fourier domain optical coherence tomography in the 2 μm wavelength range using a broadband supercontinuum source," *Optics Express* **23**(3), 1992-2001 (2015).
- [17] Jackson, S., "Towards high-power mid-infrared emission from a fibre laser," *Nature Photonics* **6**(7), 423-431 (2012).
- [18] Aubrecht, J., Peterka, P., Honzátko, P., Moravec, O., Kamrádek, M. and Kašík, I., "Broadband thulium-doped fiber ASE source," *Optics Letters* **45**(8), 2164-2167 (2020).
- [19] Pokorný, J., Moravec, O. and Aubrecht, J., "Broadband fiber-optic thulium-doped source of amplified spontaneous emission," *Proc.SPIE* **11773** (2021).
- [20] Písařík, M., Peterka, P., Zvánovec, S., Baravets, Y., Todorov, F., Kašík, I. and Honzátko, P., "Fused fiber components for "eye-safe" spectral region around 2 μm ," *Optical and Quantum Electronics* **46**(4), 603-611 (2014).
- [21] Hui, R. and O'Sullivan, M., [Fiber optic measurement techniques, 1st Edition], Academic Press, San Diego, CA (2008).

Appendix

B SPIE Optics + Optoelectronics 2023 Proceedings Article

Thulium-doped fiber amplifier optimized for wavelengths beyond 1800 nm

J. Aubrecht^a, J. Pokorný^{a,b}, B. Jiříčková^{a,b}, M. Komanec^c and Pavel Peterka^a

^aInstitute of Photonics and Electronics of the Czech Academy of Sciences,
Chaberská 57, 182 00 Prague, Czech Republic

^bFaculty of Nuclear Sciences and Physical Engineering, Czech Technical University in Prague,
Břehová 7, 115 19 Prague, Czech Republic

^c Faculty of Electrical Engineering, Czech Technical University in Prague,
Technická 2, 160 00 Prague, Czech Republic

ABSTRACT

In this contribution, we focus on development of a thulium-doped fiber-optic amplifier working in spectral range from 1800 to 2050 nm. The amplifier is core-pumped using an erbium-doped fiber laser emitting at 1565 nm with maximum output power of ~2 W. We use in-house developed and manufactured silica-based thulium-doped fibers and commercially available optical components in the setup. A tunable thulium-doped fiber laser was used as signal source allowing us to cover the whole spectral range of interest. The basic parameters of the amplifier with respect to used configuration, fiber lengths, and spectral wavelength are presented and discussed.

Keywords: Thulium, Fiber, Telecom, L-band, Silica, Fiber laser, Fiber-optic amplifier, Thulium-doped fiber

1. INTRODUCTION

Current infrastructure of telecommunication networks has almost reached its physical limits due to an exponential rise of data traffic over the last years¹. It is therefore necessary to focus on the extension of existing spectral bandwidth and try to find new, more effective solutions. The spectral regions in the E-band (1360-1460 nm) and S-band (1460-1530 nm) are being examined for use with existing fiber optic networks utilizing semiconductor optical amplifiers², alternatively the spectral region beyond the so-called L-band (1565-1625 nm) may soon become viable thanks to advancements in fiber technology^{3,4}. Optical signals at wavelengths beyond the L-band up to 2 μm can preferably be amplified by thulium-doped fiber amplifiers (TDFAs) which utilize the widest gain bandwidth amongst all rare-earth doped fibers (window from ~1750 to ~2050 nm)⁵. Currently, the optical fibers usually prepared by well-established modified chemical vapor deposition (MCVD) technology extended with solution doping technique⁶ or with ceramic nanoparticles doping⁷ can achieve a fluorescence lifetime almost 800 μs ^{8,9} and thus increase the efficiency of the fibers in applications for amplifiers or broadband sources¹⁰. TDFAs may become the key enablers in next generation telecom networks with several demonstrations confirming their viability^{11,12}. The spectral range 1800-2050 nm is also significant for applications in free-space optical communication¹³, LIDAR based gas sensing¹⁴, material processing¹⁵, polymer welding¹⁶, pumping of solid-state lasers and generation of supercontinuum¹⁷, optical coherence tomography¹⁸, defense applications¹⁹, or medical applications²⁰.

In this article, we focus on development of a TDFA working in spectral range from 1800 to 2050 nm for, in the first place, telecom applications. As the active fibers, we tested thulium-doped fibers (TDF) developed, manufactured, and drawn in-house. Based on our previous findings about the optimized fiber length and setup adjustment²¹, only amplifier parameters of the optimal setup, in terms of overall performance, are presented. A tunable thulium-doped fiber laser (TTDFL) in a Fabry-Perot configuration with a diffraction grating in a Littrow setup, used as a wavelength selective element, was used as signal source with its wide tunability allowing us to cover the whole tested spectral range. Gain, output power, and noise characteristics covering the spectral range from 1800-2050 nm are presented.

2. EXPERIMENT

We have previously demonstrated a TDFA amplifying at 1950 nm and 1996 nm, where we mainly focused on optimizing the length of the TDF²¹. We have since moved on to use a more recent TDF, which offers higher lifetimes. The gained experience was also beneficial to the development of a TTDFL that served as a signal source for the TDFA. The TDFA and the TTDFL were both core-pumped with the standard single-mode fiber (SMF28) being used in all fiber-optic components. All the presented devices employ a simple, mostly fiber geometry utilizing commercially available optical components except for the active fiber. The experimental setup used for our TTDFL is illustrated schematically in Figure 1. An in-house-built erbium-doped fiber laser (EDFL) in a ring arrangement emitting at 1565 nm was applied as an in-band pumping source for the TTDFL with a maximum output power around 1.8 W. The pump power was coupled into the active fiber by a 1560/1950 nm wavelength division multiplexor (WDM). As a gain medium we used 2 m of core-pumped highly doped (~3200 ppm Tm³⁺, 4.5 mol% Al₂O₃ concentrations) TDF which was prepared in-house using MCVD method and solution doping method. A Richardson Gratings 600 grooves/mm ruled reflection grating with a blaze wavelength of 1850 nm was used as a wavelength selective element.

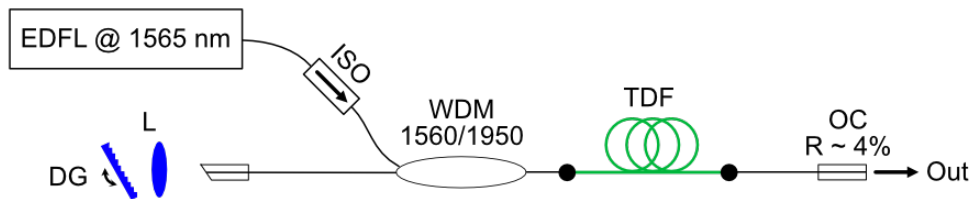


Figure 1: Experimental arrangement of the TTDFL, DG: diffraction grating, L: plano-convex lens, OC: output coupler, ISO: optical isolator.

The output power and wavelength tunability of the TTDFL were verified to ensure sufficient power and signal-to-noise ratio (SNR) available to characterize the TDFA. The output power was measured using a Thorlabs S148C integrating sphere photodiode power sensor. The PM100D Thorlabs power meter was used to display the detected power in all relevant measurements. The spectral characterization was performed using the Thorlabs OSA203C optical spectrum analyzer (OSA). We have later verified the SNR using the Yokogawa AQ 6375B OSA, which has a higher optical rejection ratio, during the gain measurements of the TDFA. The temporal characteristics of the TTDFL were also measured, using the Thorlabs PDA10D2 photodiode detector and LeCroy HDO6034 oscilloscope.

The experimental setup of the TDFA is illustrated schematically in Figure 2. The TDFA is pumped by an in-house built EDFL emitting at the wavelength of 1565 nm with a maximum output power of 2.3 W. In contrast to our earlier design²¹, we have selected a co-propagating pumping scheme primarily due to lower noise for amplification of small signals. Optical isolators on both sides of the amplifier help suppress parasitic lasing and ensure the amplifier operates in a unidirectional regime. In this case, we used a 5 m long TDF (~1700 ppm Tm³⁺, 8 mol% Al₂O₃), which was prepared in-house using the MCVD method and nanoparticle doping method⁷. Some of the optical fused components for both the TTDFL and TDFA were previously developed in collaboration with SQS Vláknová optika company²².

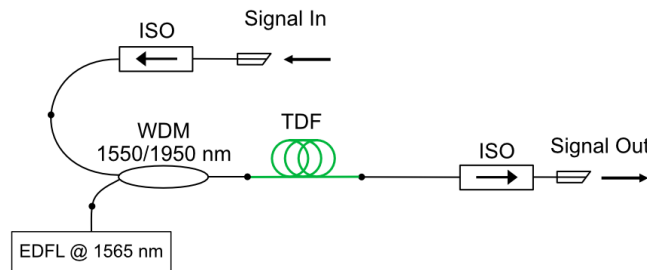


Figure 2: Experimental arrangement of the TDFA. Signal In: input signal, Signal Out: amplified signal.

The characterization of the TDFA is schematically illustrated in Figure 3. The output of the TTDFL was adjusted using a variable optical attenuator (VOA) and monitored using Thorlabs S148C at the one of the output ports of a spectrally flat

50/50 coupler, to provide signal seed for the TDFA. The output power of the TDFA was monitored at the 99% port of a 99/1 spectrally flat optical coupler by a Thorlabs S405C thermopile power detector. The second port of the coupler was used to capture the spectrum of the amplified signal. Additional calibrated attenuators were used to avoid OSA damage when deemed necessary.

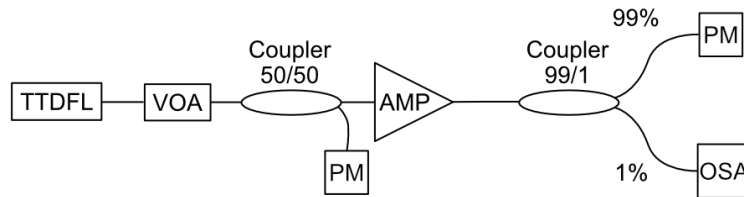


Figure 3: Experimental setup for amplifier characterization. OSA: optical spectrum analyzer, VOA: variable optical attenuator, PM: power meter, AMP: TDFA.

The gain and noise figure (NF) were determined using the automatic functions of the Yokogawa AQ6375B OSA and verified using a method, where the input and output spectral intensities are measured and then compared²³. The calculations were performed using software processing in MATLAB. A script has been developed especially for this purpose to automatically detect narrowband peaks and based on user defined parameters calculate gain and NF. As a side note, this enables the use of the Thorlabs OSA203C OSA for gain and noise figure measurement as well, albeit with limitations. The linear interpolation method was used to determine the ASE noise level. This calculation method has the added benefit of correcting the whole captured spectra for attenuation characteristics of optical components inserted between the TDFA/TTDFL and the OSA.

3. RESULTS AND DISCUSSION

The TTDFL has been found to have sufficient output power across the whole spectral range of 1800-2050 nm for the purpose of TDFA characterization. The maximum measured output power and tunability are displayed in Figure 4. Below 1810 nm the TTDFL generally suffers from parasitic lasing at longer wavelengths, which can be suppressed by either inducing temporary fiber bend loss or placing a small length of holmium-doped fiber somewhere in the laser resonator. Since this technique is performed ah-hoc and isn't well reproducible, the point is excluded from the power measurement results presented.

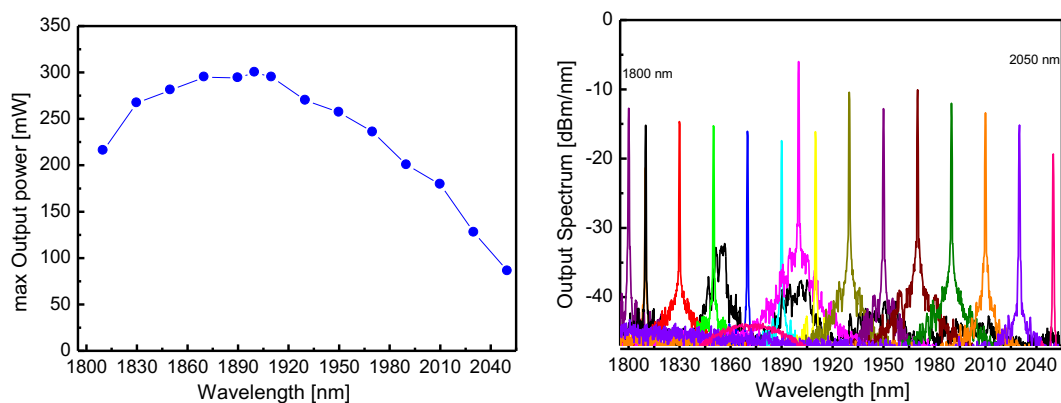


Figure 4: Left: TTDFL maximum output power versus wavelength. Right: TTDFL wavelength tunability.

The TTDFL was found to have sufficient SNR for gain and NF measurement purposes, generally exceeding the optical rejection ratio of the Thorlabs OSA203C OSA of ~44 dB for wavelengths > 6.2 nm away from the laser peak. The TTDFL operates mostly in free-running regime with occasional pulsing near the lasing threshold. The fluctuations in output power are fast enough to not influence the TDFA characterization process.

The TDFA was found to have high gain in the 1820-2020 nm spectral range. Typical examples of spectral intensities obtained from the OSA measurements using the Yokogawa AQ6375B OSA with a 0.2 nm resolution are displayed in Figure 5.

The maximum gain obtained for varying signal input power is displayed in Figure 5. Maximum small signal gain of 40.7 dB was measured at 1880 nm. A relatively flat gain spectrum of ~25 dB spanning 140 nm in the range 1840-1980 nm was observed for 0 dBm signal amplification. Those characteristics were found to be an optimal compromise between short and long wavelength operation, as amplification at shorter wavelengths requires a short fiber and vice versa. Gain outside of the 1820-2020 nm window in this configuration was considered too small for any application and not studied further.

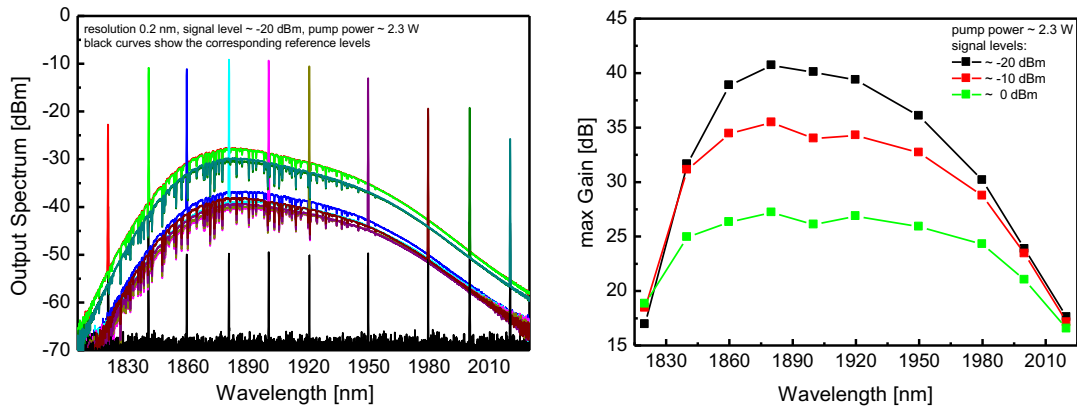


Figure 5: Left: Typical TDFA output spectra. Right: Amplifier gain characteristics versus wavelength.

The dependence of gain and NF on pump power for selected wavelengths is presented in Figure 6, left. We observe the NF staying relatively constant with increasing pump power. The gain, on the other hand, slowly saturates with increasing pump power. The NF tends to rise rapidly towards the edges of the gain spectrum, more pronouncedly on the short wavelength side, as is evident from Figure 6, right.

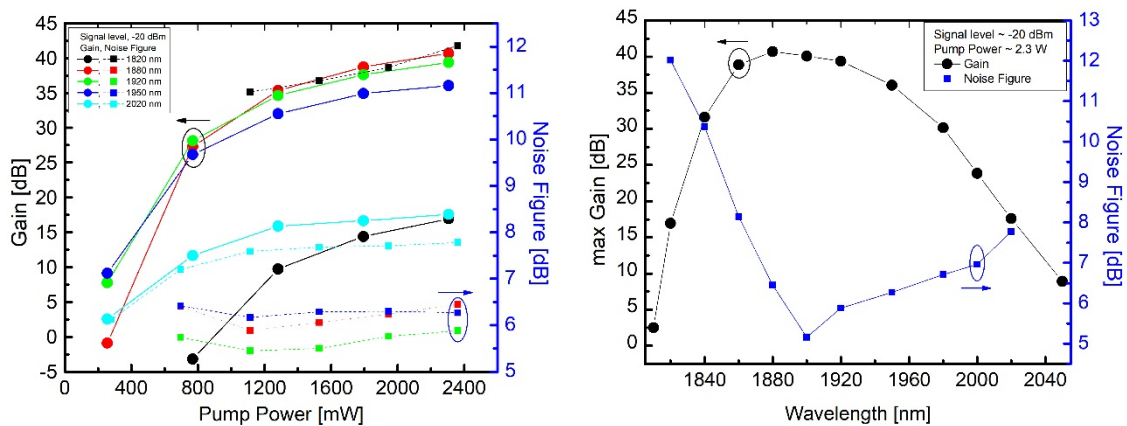


Figure 6 Gain and noise figure characteristics. Left: evolution of gain and noise figure with increasing pump power. Right: Maximum gain and corresponding noise figure at different wavelengths.

The deterioration of gain and NF characteristics at both edges of the gain spectrum can be attributed to several factors. First and foremost, the length of the active fiber plays, as previously mentioned, a crucial role in determining the gain spectrum. High population inversion is necessary for signal gain at shorter wavelengths, where the Tm^{3+} energy system exhibits strong three-level behavior, leading to strong reabsorption at the unpumped end of the TDF. Reabsorption is minimal at longer wavelengths; the Tm^{3+} emission cross section is, however, also small²⁴. This leads to longer lengths of fiber with low inversion of population achieving higher gain at longer wavelengths. These two requirements are contradictory and, as mentioned previously, a compromise was made in this case. The possibility of using counter-propagating amplified spontaneous emission to pump a short pre-amplifier section may be examined further. Secondly, the design window of optical components is limited, and insertion loss tends to increase exponentially at the edges of this window. With most of the components used having a design wavelength of either 1950 nm or 2000 nm, the insertion loss especially towards 1800 nm increases rapidly hampering both gain and NF. This issue could be solved by developing

custom optical components more suited for the gain window of the amplifier. Lastly, the attenuation and bend induced losses of the SMF28 fiber used increase rapidly at wavelengths > 2000 nm. A complete redesign of all components and the TDF for the use of a more optimized single mode fiber would be the preferred solution in this case. In the meantime, extra attention must be paid to the fiber bend radius to limit these losses.

4. CONCLUSIONS

The TTDFL for signal seeding and the TDFA for optical signal amplification were assembled using commercially available optical components and in-house made TDFs. The TTDFL offers a wide window of tunability (1810-2050 nm) and the TDFA a wide spectrum of high amplification (1820-2020 nm) with good SNR and NF, respectively. A prototype TDFA was designed, built, and characterized for a range of signal and pump powers over a large spectral window. A maximum small signal gain of 40.7 dB at 1880 nm with a corresponding noise figure of 6.45 dB was measured. Further improvements are possible provided that custom optical components with lower insertion loss designed especially for this gain window are developed. We are currently focusing on extending the spectral gain window towards 1650 nm by utilizing a novel TDF featuring a depressed cladding design, which may serve to “bridge the gap” between the existing erbium-based and thulium-based systems.

ACKNOWLEDGEMENTS

This work was financially supported by the Development Fund of CESNET under project number 672/2021.

REFERENCES

- [1] Winzer, P. J., Neilson, D. T. and Chraplyvy, A. R., “Fiber-optic transmission and networking: the previous 20 and the next 20 years [Invited],” *Opt. Express* **26**(18), 24190 (2018).
- [2] Vojtech, J., Radil, J., Havlis, O., Altmann, M., Skoda, P. and Smotlacha, V., “Resilience of semiconductor optical amplifier with holding beam injection to reflections in bidirectional reciprocal operation,” 2016 18th Int. Conf. Transparent Opt. Netw. ICTON, 1–3, IEEE, Trento, Italy (2016).
- [3] Belardi, W. and Knight, J. C., “Hollow antiresonant fibers with reduced attenuation,” *Opt. Lett.* **39**(7), 1853 (2014).
- [4] Bradley, T. D., Hayes, J. R., Chen, Y., Jasion, G. T., Sandoghchi, S. R., Slavik, R., Fokoua, E. N., Bawn, S., Sakr, H., Davidson, I. A., Taranta, A., Thomas, J. P., Petrovich, M. N., Richardson, D. J. and Poletti, F., “Record Low-Loss 1.3dB/km Data Transmitting Antiresonant Hollow Core Fibre,” 2018 Eur. Conf. Opt. Commun. ECOC, 1–3, IEEE, Rome (2018).
- [5] Agger, S. D. and Povlsen, J. H., “Emission and absorption cross section of thulium doped silica fibers” (2006).
- [6] Townsend, J. E., Barnes, W. L., Jedrzejewski, K. P. and Grubb, S. G., “Yb³⁺ sensitised Er³⁺ doped silica optical fibre with ultrahigh transfer efficiency and gain,” *Electron. Lett.* **27**(21), 1958 (1991).
- [7] Kamrádek, M., Honzátko, P., Kašík, I., Aubrecht, J., Mrázek, J., Podrazký, O., Cajzl, J., Vařák, P., Kubeček, V. and Peterka, P., “Nanoparticle and Solution Doping for Efficient Holmium Fiber Lasers,” *IEEE Photonics J.* **11**(5), 1–10 (2019).
- [8] Vařák, P., Mrázek, J., Blanc, W., Aubrecht, J., Kamrádek, M. and Podrazký, O., “Preparation and properties of Tm-doped SiO₂-ZrO₂ phase separated optical fibers for use in fiber lasers,” *Opt. Mater. Express* **10**(6), 1383 (2020).
- [9] Cajzl, J., Peterka, P., Kowalczyk, M., Tarka, J., Sobon, G., Sotor, J., Aubrecht, J., Honzátko, P. and Kašík, I., “Thulium-Doped Silica Fibers with Enhanced Fluorescence Lifetime and Their Application in Ultrafast Fiber Lasers,” *Fibers* **6**(3), 66 (2018).
- [10] Aubrecht, J., Peterka, P., Honzátko, P., Moravec, O., Kamrádek, M. and Kašík, I., “Broadband thulium-doped fiber ASE source,” *Opt. Lett.* **45**(8), 2164 (2020).
- [11] Wang, J., Liang, S., Kang, Q., Jung, Y., Alam, S. and Richardson, D. J., “Broadband silica-based thulium doped fiber amplifier employing multi-wavelength pumping,” *Opt. Express* **24**(20), 23001 (2016).
- [12] Tench, R. E., Romano, C. and Delavaux, J.-M., “Multistage single clad 2 μ m TDFA with a shared L-band pump source,” *Appl. Opt.* **57**(21), 5948 (2018).

- [13] Li, Z., Heidt, A. M., Simakov, N., Jung, Y., Daniel, J. M. O., Alam, S. U. and Richardson, D. J., “Diode-pumped wideband thulium-doped fiber amplifiers for optical communications in the 1800 – 2050 nm window,” *Opt. Express* **21**(22), 26450 (2013).
- [14] Ishii, S., Mizutani, K., Fukuoka, H., Ishikawa, T., Philippe, B., Iwai, H., Aoki, T., Itabe, T., Sato, A. and Asai, K., “Coherent 2 μm differential absorption and wind lidar with conductively cooled laser and two-axis scanning device,” *Appl. Opt.* **49**(10), 1809 (2010).
- [15] Todorov, F., Aubrecht, J., Peterka, P., Schreiber, O., Jasim, A. A., Mrázek, J., Podrazký, O., Kamrádek, M., Kanagaraj, N., Grábner, M., Baravets, Y., Cajzl, J., Koška, P., Fišar, A., Kašík, I. and Honzátko, P., “Active Optical Fibers and Components for Fiber Lasers Emitting in the 2- μm Spectral Range,” *Materials* **13**(22), 5177 (2020).
- [16] Mingareev, I., Weirauch, F., Olowinsky, A., Shah, L., Kadwani, P. and Richardson, M., “Welding of polymers using a 2 μm thulium fiber laser,” *Opt. Laser Technol.* **44**(7), 2095–2099 (2012).
- [17] Swiderski, J. and Michalska, M., “Mid-infrared supercontinuum generation in a single-mode thulium-doped fiber amplifier,” *Laser Phys. Lett.* **10**(3), 035105 (2013).
- [18] Cheung, C. S., Daniel, J. M. O., Tokurakawa, M., Clarkson, W. A. and Liang, H., “High resolution Fourier domain optical coherence tomography in the 2 μm wavelength range using a broadband supercontinuum source,” *Opt. Express* **23**(3), 1992–2001 (2015).
- [19] Jackson, S. D., “Towards high-power mid-infrared emission from a fibre laser,” *Nat. Photonics* **6**(7), 423–431 (2012).
- [20] Michalska, M., Brojek, W., Rybak, Z., Sznalewski, P., Mamajek, M. and Swiderski, J., “Highly stable, efficient Tm-doped fiber laser—a potential scalpel for low invasive surgery,” *Laser Phys. Lett.* **13**(11), 115101 (2016).
- [21] Pokorný, J., Aubrecht, J. and Peterka, P., “Broadband fiber-optic thulium-doped amplifier for wavelengths beyond the L-band,” *Micro-Struct. Spec. Opt. Fibres VII*, C.-A. Bunge, K. Kalli, and P. Peterka, Eds., 12, SPIE, Strasbourg, France (2022).
- [22] Písařík, M., Peterka, P., Zvánovec, S., Baravets, Y., Todorov, F., Kašík, I. and Honzátko, P., “Fused fiber components for ‘eye-safe’ spectral region around 2 μm ,” *Opt. Quantum Electron.* **46**(4), 603–611 (2014).
- [23] Hui, R. and O’ Sullivan, M., [Fiber Optic Measurement Techniques], Elsevier (2009).
- [24] Jiříčková, B., Grábner, M., Jauregui, C., Aubrecht, J., Schreiber, O. and Peterka, P., “Temperature-dependent cross section spectra for thulium-doped fiber lasers,” *Opt. Lett.* **48**(3), 811 (2023).

Appendix

C CLEO/Europe-EQEC 2023 Contribution

Design and characterization of thulium-doped fiber with depressed cladding for amplifiers operating in the region from L-band to 1.8 μm

Jan Aubrecht¹, Jan Pokorný^{1,2}, Michal Kamrádek¹, Bára Jiříčková^{1,2}, Pavel Peterka¹

1. Institute of Photonics and Electronics of the Czech Academy of Sciences, Chaberská 57, Prague 18200, Czech Republic

2. Czech Technical University in Prague, Faculty of Nuclear Sciences and Physical Engineering, Břehová 7, Prague 11519, Czech Republic

The current demands on optical communications are running up against their physical limits with the exponential increase in the volume of data transmitted over the Internet [1]. The increasing capacity requirements of optical transmission paths support the use of fiber amplifiers outside the standard spectral bands. For these purposes, existing aluminosilicate fibers can be used, which, unlike anti-resonant hollow-core fibers or hollow-core photonic crystal fibers, are more accessible in terms of manufacture as well as cost.

Here, we present a design and characterization of a silica-based thulium-doped optical fiber (TDF) for lasers and amplifiers operating beyond the L-band to 1800 nm region. The fiber features a depressed cladding region suppressing amplified spontaneous emission (ASE) at longer wavelengths shifting the gain towards shorter wavelengths. The behavior of the fiber was simulated through an iterative process using a combination of mode solver and beam propagation methods verifying the refractive index profile from the initial approximation to the drawn fiber, see Fig. 1a. This process also served as a form of quality check. Then, the fiber was manufactured in-house using the modified chemical vapor deposition and nanoparticle doping methods. The optimal working point of the manufactured fiber can be set by altering the bend radius of the fiber. Therefore, at first, the bending-induced losses in the fiber were characterized, and then the fiber was used as the part of a tunable fiber laser (TLS) and an optical amplifier. This procedure achieved a TLS operating point shift of more than 80 nm towards shorter wavelengths than when using an identical setup with standard TDF. In other words, our modified TLS setup thus achieved a range of tunability 1690-1800 nm as shown in Fig. 1b.

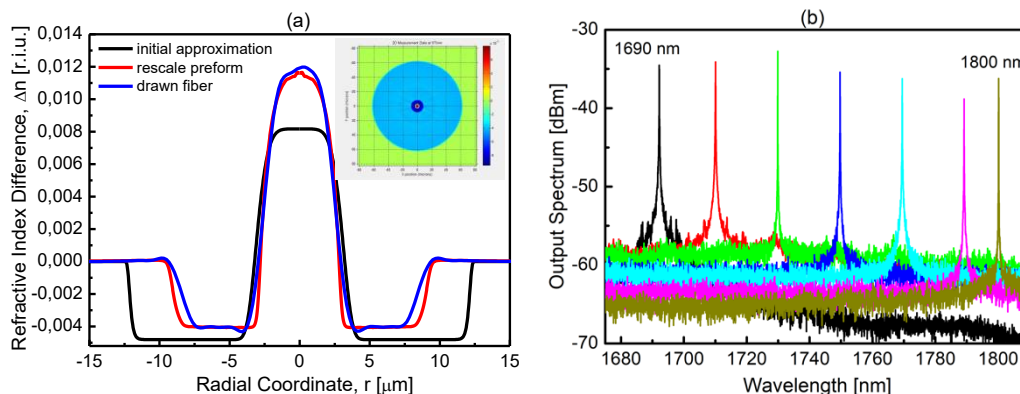


Fig. 1 a) Comparison of refractive index differences between the initial approximation, rescaling of the fabricated preform and the drawn fiber, 2-D refractive index profile in the inset. b) Individual laser peaks of the TLS using the fiber with depressed cladding.

Compared to previous solutions, which mainly used a discrete ASE filter, in the form of a section of Ho-doped fiber or a bent section of dispersion compensating fiber [2,3], a noticeable performance improvement was observed. A fiber optic amplifier based on the depressed cladding TDF using the TLS as a small-signal source was characterized and the gain enhancement at wavelengths below 1800 nm was successfully proved. This is, to best of our knowledge, the first time that a thulium-doped fiber featuring a depressed cladding has been designed, manufactured, and characterized. This work demonstrates our ongoing continuous efforts in the field of thulium-doped fiber amplifiers which evolved from the previous focus on the conventional range of 1800-2050 nm [4].

References

- [1] P. J. Winzer, D. T. Neilson, and A. R. Chraplyvy, "Fiber-optic transmission and networking: the previous 20 and the next 20 years," *Optics Express* **26**(18), 24190-24239(2018).
- [2] Z. Li et al., "Exploiting the short wavelength gain of silica-based thulium-doped fiber amplifiers," *Optics Letters* **41**(10), 2197-2200 (2016).
- [3] Z. Li et al., "Extreme Short Wavelength Operation (1.65 – 1.7 μm) of Silica-Based Thulium-Doped Fiber Amplifier," in *Optical Fiber Communication Conference*, p. Tu2C.1, OSA, Washington, D.C (2015).
- [4] J. Pokorný, J. Aubrecht, and P. Peterka, "Broadband fiber-optic thulium-doped amplifier for wavelengths beyond the L-band," *Proc. SPIE* **12140**, Micro-Structured and Specialty Optical Fibres VII, 1214009 (2022).